Scaling from individual trees to forests in an Earth system modelling framework using a mathematically tractable model of height-structured competition

E.S. Weng[1*], S. Malyshev[2], J. W. Lichstein[3], C. E. Farrior[1], R. Dybzinski[1], T. Zhang[3], E. Shevliakova[2], S. W. Pacala[1]

[1] Department of Ecology & Evolutionary Biology, Princeton University, Princeton, NJ 08544, USA

[2] Cooperative Institute for Climate Science, Princeton University, and NOAA/Geophysical Fluid Dynamics Laboratory, Princeton, NJ 08544, USA

[3] Department of Biology, University of Florida, Gainesville, FL 32611, USA

Running title: LM3-PPA model

[*] **For correspondence**

Department of Ecology & Evolutionary Biology

Princeton University

Princeton, NJ 08544

Phone: 609-258-6886

E-mail: weng@princeton.edu

Manuscript prepared for Biogeosciences (Discussion)

Abstract

The long-term and large-scale dynamics of ecosystems are in large part determined by the performances of individual plants in competition with one another for light, water and nutrients. Woody biomass, a pool of carbon (C) larger than 50% of atmospheric CO_2, exists because of height-structured competition for light. However, most of the current Earth System Models that predict climate change and C cycle feedbacks lack both a mechanistic formulation for height-structured competition for light and an explicit scaling from individual plants to the globe. In this study, we incorporate height-structured competition for light, competition for water, and explicit scaling from individuals to ecosystems into the land model version 3 (LM3) currently used in the Earth System Models developed by the Geophysical Fluid Dynamics Laboratory (GFDL). The height-structured formulation is based on the Perfect Plasticity Approximation (PPA), which has been shown to accurately scale from individual-level plant competition for light, water and nutrients to the dynamics of whole communities. Because of the tractability of the PPA, the coupled LM3-PPA model is able to include a large number of phenomena across a range of spatial and temporal scales and still retain computational tractability, as well as close linkages to mathematically tractable forms of the model. We test a range of predictions against data from temperate broadleaved forests in the northern USA. The results show the model predictions agree with diurnal and annual C fluxes, growth rates of individual trees in the canopy and understory, tree size distributions, and species-level population dynamics during succession. We also show how the competitively optimal allocation strategy - the strategy that can competitively exclude all others - shifts as a function of the atmospheric CO_2 concentration. This strategy is referred to as an evolutionarily stable strategy (ESS) in the ecological literature and is typically not the same as a productivity- or growth-maximizing strategy. Model simulations predict that C sinks caused by CO_2 fertilization in forests limited by light and water will be down-regulated if allocation

tracks changes in the competitive optimum. The implementation of the model in this paper is for temperate broadleaved forest trees, but the formulation of the model is general. It can be expanded to include other growth forms and physiologies simply by altering parameter values.

Key words: Allocation, Dynamic global vegetation model (DGVM), Evolutionarily stable strategy (ESS), Forest dynamics model, Perfect Plasticity Approximation (PPA), Plant competition, Succession, Vegetation dynamics

1 Introduction

Terrestrial ecosystems regulate biophysical exchanges of matter, energy and momentum between the atmosphere and land surface and affect long-term climate dynamics by regulating the atmospheric CO_2 concentration ($[CO_2]$; Chapin et al., 2008). Biogeochemical and biophysical interactions between terrestrial ecosystems and climate are now widely recognized as essential determinants of past and future climate change (Bonan, 2008). For this reason, global models of terrestrial ecosystems are critical, but highly uncertain, components of Earth system models (ESMs) that predict climate and climate change (Friedlingstein et al., 2006).

In most ESMs, terrestrial vegetation is simulated by a Dynamic Global Vegetation Model (DGVM; e.g., Sitch et al., 2003; Foley et al., 1996) with global plant functional diversity represented by ~10 plant functional types (PFTs; from Prentice et al., 1992). Vegetation in each model grid cell (e.g., 1° latitude × 1° longitude) is modeled as a set of pools describing different plant tissues (e.g., leaves, fine roots, sapwood, heart wood) belonging to one or more PFTs (e.g., Sitch et al., 2008; Quillet et al., 2010). Mechanistic physiological and biophysical equations govern photosynthetic carbon gain, transpiration, respiration of all plant tissues, and uptake of water and (in some models) nutrients by fine roots. Model-specific rules (often empirically derived) are used to allocate C to the different pools and to determine which PFT(s) dominate each grid cell or sub-grid tile (Sitch et al., 2003; Potter et al., 1993; Foley et al., 1996). Dead plant tissues are sent to a decomposition submodel, which usually is a variant of the CENTURY model (Parton et al., 1987). Water availability is governed by a coupled hydrological model. Some DGVMs include dynamical models of important nutrients, such as nitrogen (Thornton et al., 2007; Zaehle and Friend, 2010; Gerber et al., 2010). In fully-coupled implementations, plant canopies exchange carbon, water, energy and momentum with the atmosphere through a

82 boundary layer above the canopy air space, and roots exchange matter and energy with one or
83 more soil layers.
84 Although we have a sophisticated understanding of some important fine-scale processes
85 such as leaf-level photosynthesis, and a growing capacity to measure grid-scale fluxes and
86 storage of carbon, most current ESMs lack a set of equations that explicitly scale physiological,
87 population dynamic, and biogeochemical processes from individual plants to stands,
88 communities, and grid cells. This may contribute to the high uncertainty about C sources and
89 sinks predicted by the ESMs as revealed by model inter-comparison studies (Shao et al., 2013;
90 Todd-Brown et al., 2013; Friedlingstein et al., 2014). For example, some models predict that CO_2
91 fertilization and climate change will create a large terrestrial C sink, whereas others predict a
92 large C source, with the spread between models large relative to global anthropogenic fossil fuel
93 emissions (Friedlingstein et al., 2006).
94 Several DGVMs with explicit scaling have been developed from forest gap models
95 (Friend et al., 1997; Sato et al., 2007; Haverd et al., 2014), which have been shown to scale from
96 individual vital rates to stand dynamics with reasonable accuracy (Botkin et al., 1972; Pacala et
97 al., 1996; Shugart and West, 1977), and are thus widely used to manage forests (e.g., Coates et
98 al., 2003). Some gap models simulate height-structured competition among individual seedlings,
99 saplings, and adult trees for light, as well as competition for below-ground resources. Because
100 simulating every individual plant on Earth in this way is unfeasible, some models, such as
101 HYBRID (Friend et al., 1993; Friend et al., 1997), LPJ-GUESS (Smith et al., 2001) and SEIB
102 (Sato et al., 2007), simulate a sample of individuals in each grid cell that is small enough to
103 allow reasonable run time, but large enough to dampen random fluctuations in the underlying
104 stochastic population dynamics. An alternative approach was developed by Moorcroft et al.

105 (2001), who derived a set of integro-partial differential equations that approximately govern the
106 dynamics of the first moment of the stochastic process (the mean population density of trees in
107 the forest of each species and size) that is simulated in a gap model. Instead of averaging over
108 the many individuals in a stochastic simulation, these equations directly predict the mean
109 population densities of individuals of each species and size (height, diameter or biomass) that
110 would have been produced by a gap model of a large stand with the same functional forms and
111 parameter values. Medvigy et al. (2009) and Fisher et al. (2010) coupled the ED model into full
112 DGVMs, and several efforts are now underway to build models derived from ED into ESMs.
113 An important advantage of the DGVMs developed from gap-models, such as HYBRID,
114 LPJ-GUESS, SEIB, and ED, is that they include the mechanistic function of stem wood. Trees
115 use stem wood to overtop their neighbors when in competition for light, and to avoid being
116 overtopped by their neighbors. The wood of living trees is the largest vegetation carbon pool
117 (363±28 Pg C; Pan et al., 2011), equivalent to around half of the atmospheric carbon pool.
118 Furthermore, a large fraction of soil organic matter (SOM) comes from wood litter. It is thus
119 likely that predictions about the future of the terrestrial C sink will be improved in models that
120 include the mechanistic function of wood. For example, to determine how the terrestrial C sink
121 will change because of climate change and CO_2 fertilization, one needs to predict changes in
122 plant C allocation patterns. Because of the large difference in residence time of wood, leaves,
123 and fine roots in forests, changes in allocation can drastically change carbon sinks (Zhang et al.,
124 2010; Luo et al., 2003). Theoretically, it has been shown that under water limitation,
125 competitively optimal shifts towards greater fine-root allocation can lead to greatly diminished
126 vegetation C sinks despite significant increases in productivity (Farrior et al., 2013). Thus,
127 mechanistic predictions of whether allocation to wood will increase, decrease, or stay the same,

under the altered environmental conditions are critical. However, competitively optimal plant allocation has not, to our knowledge, been rigorously studied in any of the previous gap-model-derived DGVMs.

Despite the advantages of gap-model DGVMs, it is difficult to understand the behavior of these models because they are analytically intractable even under idealized conditions, such as constant climate, and so can only be studied using numerical simulations. For example, competitively optimal plant C allocation could only be studied in these models by relying on computational experiments that may be difficult to interpret in the absence of any theoretical guidance. The price of added complexity in a DGVM is that it increases the number of ways in which model errors can interact and cause misleading predictions (e.g., model equifinality), which are especially difficult to diagnose and understand if one cannot study the model analytically. This problem is particularly acute when developing an ESM, which has many interacting components. For this reason, height-structured competition was not included in the GFDL land model version 3 (LM3) (Shevliakova et al., 2009; Milly et al., 2014).

In this paper, we present a new, biodiverse version of LM3 that includes height-structured competition among plants for light, as well as competition for water. Future versions will include competition for nitrogen and phosphorus. The new model, LM3-PPA, is based on the Perfect Plasticity Approximation (PPA), a computationally simple and mathematically tractable model that scales from individuals to stand dynamics (Strigul et al., 2008). Like ED, the PPA allows one to derive integro-partial differential equations for the first moment of the stochastic process that defines an individual-based forest model (Strigul et al., 2008). But, unlike ED, these equations are analytically tractable under idealized conditions (e.g., constant climate). The PPA model closely matches the behavior of stochastic individual-based forest dynamics

models (gap simulators; Strigul et al., 2008). More importantly, it has been shown to predict species-level succession across different soils in the USA Lake States (Purves et al., 2008) and to accurately predict canopy structure in temperate and tropical forests (Bohlman and Pacala, 2012; Purves et al., 2007; Zhang et al., 2014). Dybzinski et al. (2011; 2013) and Farrior et al. (2013) have developed game theoretic versions of the PPA that use analytical methods to identify the most competitive allocation strategy (investment in fine roots, wood, and leaves) of trees competing for light, water, and nitrogen. Although these game theoretic models are physiologically simpler than most DGVMs, they yield quantitatively accurate predictions of net primary production (NPP) and plant allocation observed at Fluxnet sites (Luyssaert et al., 2007). These theoretical studies have guided the development of the new DGVM presented here, LM3-PPA.

Although the fast time-scale processes in LM3-PPA (e.g., exchanges of energy and matter between vegetation, atmosphere, and soil) render it analytically intractable, its close association with the stand-alone PPA model allows for a greater understanding of model behavior than is possible with other gap-model DGVMs, including how competition for multiple resources is expected to affect allocation of NPP among different plant tissues. Variation among individuals, species, or PFTs in how carbon is allocated to leaves, wood, fine roots, etc. is recognized as a key feature of next-generation DGVMs that aim to represent plant functional diversity (both within and between model grid cells) more accurately than the current suite of models (Scheiter et al., 2013; Wullschleger et al., 2014). LM3-PPA was specifically designed with allocational and other aspects of plant functional diversity in mind.

In particular, we developed LM3-PPA to:

1) include the influence of height-structured competition for light on forest dynamics and dominant allocation strategies,
2) improve the representation of feedbacks that alter ecosystem-level allocation to wood,
3) include within-PFT biodiversity by allowing for multiple, competing variants or "species" that differ in their allocational strategy or other traits,
4) improve the scaling from individuals to landscapes using macroscopic equations from the literature on individual-based forest models, and
5) provide a global land model that can be solved analytically in idealized cases (e.g., constant climate).

In what follows, we first present the equations that underpin the LM3-PPA model in their continuous (in time and plant size) form. The numerical machinery that is necessary to discretize and implement the model as a component of an ESM is described in technical appendices (A and B). The model structure allows for an arbitrary number of "species" (broadly defined to include different genotypes or PFTs), that may have fixed or plastic parameter values describing their physiological properties and how they allocate available carbon. We evaluate the model's behavior at a series of organizational scales in a temperate forest: physiological (photosynthetic carbon gain), individual (stem diameter and height growth rates), population (size structure and population densities), community (species-level successional dynamics) and ecosystem (C storage, NPP); and at a series of temporal scales: diurnal, seasonal, interannual and centennial. We also introduce a prototype algorithm for determining the most competitive allocation strategy (i.e., the evolutionarily stable strategy, ESS) within a functional type. We use this ESS algorithm to evaluate the expected shift in C allocation between fine roots and woody tissues caused by the leaf-level water use efficiency benefits of CO_2 fertilization and the impact of this shift on the predicted C sink.

2 Model Description and Simulation Tests

2.1 The Coupled LM3-PPA Model

Consider a spatial stochastic forest model in which each tree is represented as a discrete individual with *x* and *y* coordinates, stem diameter, height, biomass, crown area, leaf area per unit crown area (crown LAI), and fine root biomass. These individuals intercept light, shade smaller individuals in their vicinity, and take up soil water. The resulting fixed C, in excess of respiration costs, is allocated to new tissues, and so the plants grow and produce seeds. Individuals also die because of random events, such as windthrow, and suffer competitive mortality because of light and/or water shortage. Finally, seeds disperse and produce new seedlings. The model predicts the size-structured dynamics of each species (or PFT, etc.) by predicting the fate of each and every individual.

This spatial stochastic process is analogous to the dynamics of the atmosphere resulting from the stochastic movement of every gas molecule. In the same way that one can derive the Navier Stokes equations from the stochastic process of molecular motion, it is possible to derive equations for the mean population densities of trees from a stochastic gap model. But because gap models are highly nonlinear, approximations must be used. One impediment to a tractable approximation has been the lack of a mechanistic and compact way of representing how the irregular spatial distribution of stems, which strongly affects the outcome of competition, results in a nearly continuous leaf canopy, which strongly affects gas exchange. ED, like the stochastic models from which it was derived (Shugart, 1984; Botkin et al., 1972), does so by simply partitioning space into adult-tree-sized cells and assuming that each individual's crown covers all the area in its cell (Moorcroft et al., 2001). As there can be many individuals per cell, there can

220 be many overlapping canopies, and any tree that is not the tallest in the cell is not in full sun. The
221 problem with this assumption is particularly evident in recently-disturbed gaps, which in reality
222 may contain multiple trees that are all in full sun.

223 In the forest gap simulator from which the PPA is derived (SORTIE with plastic crown
224 shapes due to phototropism; Strigul et al., 2008), the crown of an open-grown tree of height Z is
225 an envelope of leaves whose shape is defined by a function $A(Z',Z)$ that gives the crown area
226 above height Z'. The potential crowns of trees in a closed-canopy forest overlap so that, from
227 above, the canopy looks like a patchwork of non-overlapping territories, with each territory
228 being the portion of a canopy tree's crown that is in the sun (Mitchell, 1969). Strigul et al. (2008)
229 studied the statistics of the places where the potential crowns of adjacent canopy trees join and
230 showed that if tree growth was realistically plastic because of mild phototropism of apical
231 meristems, then the standard deviation of these canopy-crown join-heights is an order of
232 magnitude smaller than the mean join height. They derived approximate equations, taken in the
233 limit of zero crown-join-height standard deviation, for the time evolution of the first moments of
234 the stochastic process in the gap simulator; i.e., the function $N_i(s,t)$ for each species-i in the
235 model, which gives the expectation of a species' population density for individuals of size s at
236 time t. The derivation of these means used only the individual-level information in a gap
237 simulator and thus scales from individual to stand. The approximation is called the Perfect
238 Plasticity Approximation (PPA) because it is derived from the limit of extreme flexibility of
239 crown shape in the horizontal by trees in pursuit of light.

240 The PPA equations are a special case of a general size-structured demographic model
241 governing the time evolution of the population density of individuals of species-i and size s,
242 $N_i(s,t)$ (Strigul et al., 2008; von Foerster, 1959). One should think of $N_i(s,t)$ as the mean

243 population density of individuals per unit ground area in a stochastic gap model. It is the limit of
244 the expectation of $n_{ist}/(\delta_s \delta_x \delta_x)$ as δs and δx approach zero, where n_{ist} is the number of individuals
245 of species-i with size between s and $s+\delta s$ at time t in a randomly chosen quadrat with ground
246 area $(\delta x)^2$ in runs of a stochastic individual-based forest model (Strigul et al., 2008). In reality
247 and in most of this paper, the size (s) of a tree is a vector describing its height, crown area, tissue
248 pool sizes, etc. But for the moment, consider the simple case where there is only a single
249 measure of size. The system of equations governing the time evolution of $N_i(s,t)$ is usually
250 written as a system of nonlinear advection equations (advection in s) with a boundary condition
251 governing the recruitment of new individuals at the smallest size (Moorcroft et al., 2001; Strigul
252 et al., 2008). But we write them here in a mathematically equivalent form as implemented in the
253 LM3-PPA code.

254 **Population dynamics.** LM3-PPA makes population dynamics predictions by simply
255 simulating the birth, mortality, and growth of each age cohort of plants. The cohorts within the
256 same place (tile within a grid cell, see Appendix A) interact with one another only indirectly by
257 affecting resources levels – canopy trees shade understory trees, and all cohorts reduce available
258 water. In addition, cohorts in the same place have indirect biophysical impacts on one another
259 because they jointly affect the temperature and humidity of the sub-canopy airspace. These
260 indirect effects are explained in later sections and a series of Appendices. Here, we describe the
261 population dynamics assuming that the resource levels and biophysical conditions affecting a
262 cohort are known. For each species (or PFT) i, the equation that governs the density of a cohort
263 when it is born is:

$$N_{it}(t) = \int_0^t N_{i,t-\tau}(t) F_i\left(s_{i,t-\tau}(t), t\right) d\tau \qquad (1)$$

where $N_{ib}(t)$ is the population density at time t of individuals *in the same age cohort* (species-i individuals at time t who were born at time b), and $N_{it}(t)$ is the density of newborns at the time of their birth (when $b = t$); $s_{ib}(t)$ is the size at time t of individuals born at time b; and $F_i(s,t)$ is the rate of new seedling production at time t for an individual of species i and size s. Eq 1 simply sums the reproductive output of all cohorts of a given species to produce the initial density of the new cohort born at time t. We also need an equation for the loss of individuals in each cohort as it ages. After being born, individuals die at rate $\mu_i(s,t)$:

$$\frac{dN_{ib}(t)}{dt} = -\mu_i\left(s_{ib}(t),t\right)N_{ib}(t) \qquad (2)$$

Finally, we need an equation for the growth of individuals in each cohort. If $g_i(s,t)$ is the growth rate of individuals of species i and size s at time t, then:

$$\frac{ds_{ib}(t)}{dt} = g_i\left(s_{ib}(t),t\right) \qquad (3)$$

Eqs 1-3 provide an efficient way to solve the model numerically, because one can simply discretize b and thus yield a set of ordinary differential equations that have much greater numerical stability than advection equations. The LM3-PPA model uses this numerical method and thus simulates a discrete number of cohorts.

To convert Eqs 1-3 into the measures we need for a DGVM, we first divide each individual into 5 separate tissues or carbon (C) pools (leaf, fine root, sapwood, heartwood, and non-structural carbohydrates; Fig. S1 in Supplemental materials) and introduce allometric relationships to calculate the amounts of C in these five pools, as well as other measures of size, from three quantities: stem diameter ($D(t)$), crown LAI ($l(t)$; leaf area per unit crown area), and carbon in the non-structural carbohydrate pool ($NSC(t)$). Stem diameter and crown LAI were chosen because these are easily observable, and $NSC(t)$ because all plant carbon starts as non-

structural carbohydrate. In this paper, stem diameter is assumed to equal diameter at breast height (DBH) in any comparisons with DBH data. With the three measures of size, s, the right hand sides (RHS) of Eqs (1-3) each become three separate equations - one for each measure of size. Also, because each cohort has a size vector, it is always possible to calculate the density of a species or PFT as a function of any measure of size, rather than as a function of birth date. In what follows, we switch to size-structured densities, $N_i(s,t)$, whenever convenient.

Vertical and horizontal spatial structure. Again, each cohort in LM3-PPA belongs to a species (or PFT, etc.) and has three time-evolving measures of size: stem diameter, $D(t)$, crown LAI, $l(t)$, and amount of carbon in the non-structural carbohydrate pool, $NSC(t)$. We sometimes omit from the notation the time-dependence from $D(t)$, $l(t)$, and NSC(t), to keep the formulae easy to read. These measures are related to other important measures of size by species- or PFT-specific allometric relationships. Height, $Z(D)$, wood carbon mass, $S(D)$ (including stem, branches, and coarse roots), and total crown area, $A_{CR}(D)$, are functions of diameter:

$$Z(D) = \alpha_Z D^{\theta_Z}$$
$$S(D) = 0.25\pi\Lambda\rho_W\alpha_Z D^{2+\theta_Z} \qquad (4)$$
$$A_{CR}(D) = \alpha_c D^{\theta_c}$$

where α_c, α_Z, Λ, and ρ_W (wood carbon density; kg C m^{-3}) are species- or PFT-specific constants; and θ_c and θ_Z are constant across species/PFTs (1.5 and 0.5 respectively), though these could be made species/PFT-specific if necessary. A cohort's total leaf mass, $L(D, l)$, is its total leaf area ($l \times A_{CR}$) times its species- or PFT-specific leaf mass per area, LMA, and − following the pipe model (Shinozaki et al., 1964) − fine root carbon mass, $FR(D, l)$, and sapwood cross sectional area, $A_{sw}(D,L)$, are proportional to total leaf area:

$$L(D,l) = lA_{CR}(D)LMA$$

$$FR(D,l) = \varphi_{RL} lA_{CR}(D) / SRA \qquad (5)$$

$$A_{SW}(D,l) = \alpha_{CSA} lA_{CR}(D)$$

where φ_{RL}, SRA, and α_{CSA} are species/PFT-specific constants: φ_{RL} is the ratio of total root surface area to the total leaf area, SRA is specific root area, and α_{CSA} is an empirical ratio of target leaf area to sapwood cross-sectional area. Unless otherwise stated, units are: mass=kg C, area=m^2, height=m, and diameter=m. All other size measures of structural pools can be calculated from these quantities. For example, heartwood carbon mass is: $S(D) - A_{sw}(D,l)Z(D)\Lambda\rho_W$.

Fine root spatial structure. Because the area covered by a tree's root distribution is significantly larger than its crown area (Hruska et al., 1999), we assume that roots of competing individuals are uniformly distributed in the horizontal plane (Dybzinski et al., 2011 and refs therein). LM3 and LM3-PPA can be configured with an arbitrary number of vertical soil layers, with 20 layers in this study (see Appendix B for details). Each species or PFT has an empirical exponential depth distribution for its fine roots (Appendix B).

Canopy structure. A critical quantity in the PPA model is the crown join height that separates the upper canopy from the understory Z_1*:

$$k(1-\eta) = \sum_i \int_{Z_k^*}^{\infty} N_i(Z,t) A_i(Z_k^*, Z) dZ \qquad (6)$$

where k=1 for the top canopy layer, η is the proportion of each canopy layer that remains open due to spacing between individual tree crowns, $N_i(Z,t)$ is the density (m^{-2}) of trees of species i with height Z, and $A_i(Z_k^*, Z)$ is the area (m^2) of the portion of a tree's crown at a height greater than or equal to Z_k*. If the right hand side (RHS) of Eq 6, the collective crown area of all trees per unit ground area, is less than the fraction of ground area that could potentially be filled (1-η)

even for $Z_1^* = 0$, then plant density is too low to close the canopy. However, if the Z_1^* that solves Eq 6 is greater than zero, then the trees close the canopy, by definition filling the canopy with the sun-exposed portion of the crowns of individuals taller than Z_1^*. Plants that are shorter than this value, Z_1^*, are in the understory. In many temperate and boreal forests, the potential crowns of all individuals add up to less than two (do not fill a second canopy), and so Eq 6 has no solution for $k>1$. However, in some forests (e.g., tropical rainforests, and temperate forests with multiple understory layers), the sum of the crown areas of all individuals combined is typically 3 to 4 times the land area (Bohlman and Pacala, 2012), in which case Eq 6 defines a Z_2^* separating the first full understory from the second understory beneath it, a Z_3^* separating the second from the third understory, and so on.

Mathematical and computational tractability is greatly facilitated in the PPA model by the assumption that trees have flat-topped crowns (Strigul et al., 2008), which allows for accurate predictions of observed succession and canopy structure in broad-leaved temperate forests (Purves et al., 2008; Zhang et al., 2014) and vital rates and canopy structure in a Neotropical forest (Bohlman and Pacala, 2012). With a flat-topped crown, all the leaves of a tree are assumed to be in one layer, either in the upper canopy or in a single understory layer (Fig. A1 and Fig. S1a). We assume flat tops in LM3-PPA and thus use $A_{CR}(D)$ as the sole measure of crown area; i.e., $A_i(Z',Z(D)) = A_{CR}(D)$ for all $Z' \leq Z(D)$. Each cohort in LM3-PPA (and all of its leaves) belongs to exactly one canopy layer. Again, the upper canopy layer includes the tallest cohorts of trees whose collective crown area sums to the fillable ground area ([1-η] times the ground area; or less than this area if the canopy is not closed; Eq 6). Trees within the same layer do not shade each other. The trees in each understory layer are shaded by the leaves of all taller canopy layers (Appendix B). In LM3-PPA, the assumption of flat-topped crowns introduces a potential

problem that does not occur in simpler versions of the PPA model that lack physiological mechanisms. Specifically, the NSC pool can, in some cases, be quickly consumed when a tree enters the upper canopy from the understory because of the sudden increase in target leaf and fine-root biomasses. This increase would be more gradual with other crown shapes (e.g., rounded). To address this problem (which we view as a model artifact), we introduced a parameter to limit the rate of increase of target leaf mass (and therefore fine-root mass, given the pipe-model constraint) for cohorts that recently entered the upper canopy (see Eq A6 in Appendix A).

Fast time-scale exchanges of matter, energy, and momentum. Like other land models that are fully coupled to atmospheric models, LM3-PPA computes fluxes of matter, energy, and momentum between a plant's surface and the bottom of the boundary layer in the atmosphere on the fast time scale of the atmospheric model (e.g., every thirty minutes in most implementations of LM3 and LM3-PPA). This requires a network of interacting equations that are similar among many land models, including:

(i) Energy and mass balance equations that govern leaf, canopy air and soil temperatures, canopy vapor pressure deficit (VPD), wind speed in the canopy air space, and long- and shortwave radiation transfer.

(ii) A photosynthesis model at the leaf level.

(iii) A model of respiration for all plant tissues.

(iv) A model of stomatal conductance and fine-root water uptake.

(v) A model of soil water dynamics.

(vi) A model of the decomposition of soil organic matter.

366 The fast time scale equations are described in Appendix B. They are identical to those in
367 the version of LM3 used in the ESMs of GFDL (Dunne et al., 2012; Dunne et al., 2013), except
368 for a few key differences. First, whereas LM3 has only a single cohort in any one place, LM3-
369 PPA has a multi-cohort canopy and fine root distribution that (a) can be composed of more than
370 one species/PFT, (b) may have one or more complete understory canopies, and (c) always has a
371 partially full lowest understory layer if it has one or more full canopies. Second, the respiration
372 parameterization for sapwood has been updated in LM3-PPA. Observations show that the
373 respiration rate of sapwood per unit of biomass decreases with sapwood biomass (Ryan et al.,
374 2004). Consistent with these observations, LM3-PPA assumes that respiration of sapwood is
375 proportional to crown area, $A_{CR}(D)$.
376 LM3-PPA handles radiation transfer through the crowns of each cohort in the same way
377 that LM3 handles transfer through its single canopy. Radiation emanating from the bottoms of
378 crowns in the same canopy or partial canopy layer is summed before hitting the next layer or the
379 ground. All other calculations are made separately for each cohort, and summed where necessary.
380 For example, sensible and latent heat fluxes from the leaves of each cohort into the sub-canopy
381 airspace are summed in the energy balance for the air space. Appendix B documents the details
382 of the fast-time scale calculations in LM3-PPA.
383 **Growth and reproduction.** In this section, we briefly describe the fecundity function (F)
384 in Eq (1) and the growth functions on the RHS of Eq (3) for stem diameter, $D(t)$, crown LAI, $l(t)$,
385 and amount of carbon in the non-structural carbohydrate pool, $NSC(t)$. The derivations and
386 detailed discussion of these expressions are in Appendix A.
387 The carbon fluxes from the fast time scale equations (Appendix B) are summed over the
388 diurnal cycle, to provide daily total carbon gain from photosynthesis, $P_s(t)$, and loss from

389 respiration, $R_a(t)$, for each cohort. This carbon is added to or taken from the cohort's NSC pool
390 once a day:

391 $$\frac{dNSC}{dt} = P_s(t) - R_a(t) - G_{L+FR}(t) - G_{W+F}(t) \qquad (7)$$

392 where $G_{\mathrm{L+FR}}(t)$ is the amount of carbon allocated to produce new leaves and fine roots minus the
393 carbon retranslocated from senescing leaves and fine roots, and $G_{\mathrm{W+F}}(t)$ is the carbon allocated to
394 stem and seed production.

395 Expressions for $G_{\mathrm{L+FR}}(t)$ and $G_{\mathrm{W+F}}(t)$ are derived in Appendix A. The derivations assume
396 that a plant allocates carbon so that the LAI within its crown tracks a species- or PFT-specific
397 target. This target crown-LAI differs between understory and canopy individuals and seasonally
398 because of a phenology function, $p(t)$, which is unchanged from LM3, except that it is updated
399 daily rather than once per month as in LM3 and LM3V (Shevliakova et al., 2009; Milly et al.,
400 2014). Individuals also have a target root area per-unit crown area, which is equal to the target
401 crown LAI multiplied by φ_{RL} (the ratio of total root surface area to total leaf area; see Eq 5).
402 Finally, there is a target ratio of wood to seed production, and a species- or PFT-specific NSC
403 target, which scales with target leaf mass and tracks a plant's phenological state (Eq A2.4 in
404 Appendix A).

405 Our formulation for $G_{\mathrm{L+FR}}(t)$ assumes that positive net production, $P_s(t) - R_a(t)$, is
406 allocated first to leaves and fine roots if these are beneath their target levels. Carbon is
407 retranslocated back to NSC if leaves are above target (i.e., at the end of the growing season, or if
408 a cohort falls into the understory from the overstory). Carbon is allocated to wood and seeds
409 from NSC only if NSC is above its target level. The formulation also includes parameters that
410 limit the maximum rate at which NSC can be converted into leaves and fine roots and wood.

411 Appendix A shows how the assumptions about allocation can be combined with the
412 allometric equations (Eqs 4-5) to produce differential equations for the growth of stem diameter
413 and crown LAI. All other measures of plant size (e.g., fine root mass or leaf mass) can be
414 calculated from NSC, diameter, and crown LAI using the allometric equations.

415 **Mortality and disturbance.** In this section, we specify the mortality functions on the
416 RHS of Eq (2). Mortality in the PPA reduces the population density of a cohort (i.e., by a
417 fraction $\mu\delta t$ in a time-step δt if the individual mortality rate is μ). In LM3-PPA, mortality is
418 assumed to occur due to carbon starvation if a cohort's NSC pool falls to zero. Because the target
419 size of the NSC pool is assumed to be several times the size of the combined target leaf and fine-
420 root masses (see Eq A2.4 in Appendix A), trees rarely die of carbon starvation unless they
421 experience prolonged drought (which was not simulated in the current study) or have chronic
422 negative carbon balance due to shading. In addition to carbon starvation, each species/PFT has a
423 canopy-layer-specific background mortality rate that is assigned from the literature (Runkle,
424 2000). These background rates are assumed to be size-independent for upper-canopy trees (μ_{C0}
425 in Table 1), but size-dependent for understory trees according to:

426 $$\mu_U = \mu_{U0}\frac{1+10e^{-30D}}{1+2e^{-30D}} \qquad (8)$$

427 This functional form reduces mortality by a factor of 5 between germination and adulthood (Fig.
428 1a). It accounts for the additional sources of non-starvation mortality facing small individuals,
429 including herbivory by large mammals and branch-fall.

430 For all canopy layers, the background mortality rate is assumed to be independent of the
431 physiological state of the focal individual and the density of competing individuals, as these
432 physiological and competitive effects are already accounted for by mortality due to carbon

433 starvation. We also evaluated an alternative assumption for canopy trees in this paper, in which
434 the mortality rate of large trees increases with size (see Section 2.2.2 below).
435 Stand-level disturbances (e.g., due to insect outbreaks, windstorms, fire, or land use) may
436 be implemented in LM3-PPA using the land-use tiling scheme described below and in Appendix
437 A, but were not implemented in the simulations presented in this paper.
438 **Grid structure, sub-grid-scale heterogeneity, and relation to LM3.** Like LM3, LM3-
439 PPA is implemented on a flexible grid, whose cell size can be specified independently of the
440 atmospheric model's grid. LM3-PPA also includes LM3's dynamic tiling scheme for land use,
441 stand-level disturbance, and subgrid-scale heterogeneity (Shevliakova et al., 2009). As explained
442 in Appendix A, the tiling scheme can be used to implement the ED approximation for canopy
443 gap dynamics (Moorcroft et al., 2001), but this feature was not used in the simulations presented
444 in the current paper.
445 The critical difference between LM3 and the LM3-PPA model described in this paper is
446 that each tile in LM3-PPA can contain an arbitrary number of cohorts who compete with one
447 another for light and water. Each cohort belongs to a single species or PFT, but different cohorts
448 within the same tile can be from different species/PFTs. Thus, there is competition for light and
449 water among cohorts belonging to the same species/PFT (intraspecific competition), as well as
450 among cohorts belonging to different co-occurring species/PFTs (interspecific competition).
451 Coexistence of multiple species/PFTs is not assumed, but rather is a possible emergent outcome
452 of the individual-level processes that determine the community dynamics.
453

454 **2.2 Model evaluation and simulation tests**

455 The model was evaluated in temperate deciduous forest in Wisconsin, USA. A variety of data are
456 available in this region to evaluate the model's behavior, including forest inventory data from the
457 U.S. Forest Inventory and Analysis (FIA) database (http://www.fia.fs.fed.us/), biometric data
458 (Curtis et al., 2002), and eddy-covariance data (Desai et al., 2008). Furthermore, there are clear
459 patterns of forest succession among some of the dominant tree species in the region (see below),
460 which facilitates tests of predicted successional dynamics. Meteorological inputs were extracted
461 from the Sheffield et al. (2006) 1° latitude × 1° longitude, three-hourly, 1948-2008 climate
462 reanalysis data set for the grid cell containing the Willow Creek Ameriflux site (Desai et al.,
463 2008). We forced the model with the Sheffield reanalysis data rather than the meteorological
464 data from the Ameriflux site because some model tests (e.g., forest size structure and
465 successional chronosequences) were performed at a regional scale (see details below).

466 Models such as LM3-PPA are inevitably tuned during development so that they
467 reproduce realistic behavior. We tuned physiological aspects of the model (photosynthesis,
468 respiration, and NSC dynamics) to produce the observed magnitude of NPP, and a single
469 parameter affecting diameter growth rates (the taper constant, Λ). We also tuned the size-
470 dependence of background mortality (Fig. 1a) for small seedlings and saplings to reconcile large
471 observed abundances of germinating seedlings with low observed abundances of saplings. We
472 did not tune emergent behaviors such as differences among the growth rates of canopy and
473 understory trees, differences among the growth rates of trees of different species, population
474 densities of individuals above 0.1 m in diameter, successional turnover, and patterns of carbon
475 storage. In what follows, comparisons of predicted and actual NPP should be viewed as
476 demonstrations that the model is capable of exhibiting realistic behavior, because physiological

aspects of the model were tuned. However, comparisons involving variation among individuals in whole-tree growth rates, population densities and size structure for individuals above 0.1 m in diameter, and successional and ecosystem dynamics should be viewed as tests of emergent predictions of the model.

2.2.1 One- vs. three-species simulations

We implemented the model with three tree species − trembling aspen (*Populus tremuloides* Michx.), red maple (*Acer rubrum* L.), and sugar maple (*Acer saccharum* Marsh.) – to evaluate the model's capacity to capture successional dynamics and to quantify how successional diversity affects model behavior compared to one-species simulations. The three species are common in eastern North America and at the Willow Creek site in particular, and they differ in their successional status and shade tolerance (Burns and Honkala, 1990): trembling aspen is a pioneer species with high growth rate, high mortality rate, and low shade tolerance; sugar maple is a late successional species with low growth rate, low mortality rate, and high shade tolerance; and red maple is an intermediate species. These three species are not intended to fully characterize the Willow Creek or other temperate tree communities, and in this paper we do not attempt to determine the optimal number of species or functional types for ESM applications. In addition to the three-species simulations designed to evaluate successional dynamics and perform model-data comparisons at Willow Creek, we also performed a series of competition experiments with multiple functional variants defined by their allocational strategy (see Section 2.3, below) as an initial exploration of an axis of functional variation that could be incorporated into future global applications. We estimated model parameters for the three Willow Creek

499 species using data from the literature (Table 1). Most of the other parameter values (Table 1 and
500 Tables C1- C3 in Appendix C) were taken directly from LM3.
501 We compared carbon and population dynamics of runs with one species (sugar maple)
502 and all three species. Simulations were initialized with a number of small seedlings for each
503 species (Table 1 and C4) and run for 1000 years. Runs simulating species succession were
504 initialized with abundances and size distributions of each species from early-successional FIA
505 plots (plots less than 10 years of age, Table C4). We examined model predicted population
506 densities; size distributions; annual GPP and NPP; growth rates of diameter at breast height
507 (DBH), foliage biomass, stems, and fine roots; and total C storage.
508 We compared model output both to published data of GPP, NPP, plant DBH growth rates,
509 and forest composition at the Willow Creek Ameriflux site and to FIA data on mesic soils from
510 the Laurentian Mixed Forest Ecoprovince (Cleland et al., 2007), which spans northern Michigan,
511 Wisconsin, and Minnesota, USA and includes the Willow Creek site. Hereafter, we refer to this
512 ecoprovince as the "northern Lake States". Each FIA plot includes measurements on only 0.067
513 ha distributed over a 0.4 ha area; thus, data from many plots must be aggregated by stand age
514 class to estimate successional patterns of biomass, density, and size distribution.
515
516 **2.2.2 Sensitivity of LM3-PPA to alternative assumptions: mortality, allometry, and gap-**
517 **dynamics**
518 Runs of LM3-PPA predict realistic size distributions for a few hundred years of succession, but
519 produce unrealistically large trees in old growth forests (see results below). Although there are
520 only a few unrealistically large trees, they are so large that they store considerable carbon and
521 skew predictions. We have encountered this problem before when working with forest gap

522 simulators (e.g., SORTIE; Pacala et al., 1996), and we hypothesize two possible causes. First,
523 although LM3-PPA assumes constant size- and density-independent death rates of canopy trees
524 (aside from carbon starvation, which rarely occurred for canopy trees in the simulations
525 presented here), many studies have documented increased mortality as trees become very large
526 (Runkle, 2000). Xu et al. (2012) found that increases in mortality rate could explain the declining
527 rate of biomass accumulation in an old growth temperate forest. We thus compared **H0**, the
528 baseline LM3-PPA model with constant canopy tree mortality rates, with **H1**, the same model
529 with upper-canopy mortality rates that increase with tree size as shown in Fig. 1a. Second, the
530 allometry and respiration assumptions in LM3-PPA predict that a canopy tree's DBH growth rate
531 increases monotonically to an asymptote as a tree becomes large. This prediction is supported by
532 dendrochronological studies for the first one or two centuries, but actual growth rates
533 subsequently decline in very old trees (Sillett et al., 2010). We compared output from **H0** and **H2**,
534 in which DBH growth rates decline for very old trees, as reported in dendrochronological studies.
535 Rather than prescribing an arbitrary growth curve, the DBH growth rate decline results from a
536 modified crown-area allometry in **H2**, in which crown area becomes constant after a tree reaches
537 0.8 m in DBH (C. Canham, unpublished data), rather than continuing to increase with diameter
538 according to the crown area allometry in **H0** (see Eq 4). The modified allometry in **H2** results in
539 declining DBH growth rate for DBH > 0.8 m because leaf area (and thus potential C gain)
540 plateaus. All else equal, this causes sapwood volume growth to plateau, which causes decreasing
541 diameter growth (because the volume is "stretched" around a growing circumference and along
542 an increasing height).
543 Finally, the mathematical approximation behind the PPA leads to a sharp separation
544 between canopy and understory; i.e., a single height at any one time separating all canopy trees

from all understory trees in a given stand (or subgrid cell tile in LM3-PPA). The PPA thus predicts that old growth recruitment into the canopy comes exclusively from saplings that have spent a long time in the understory (advance regeneration). While this is true for shade tolerant species, it is not true for pioneers that exploit large gaps in old growth forests. Section 5 of Appendix A describes how the subgrid-scale tiling scheme in LM3-PPA could be used to simulate gap dynamics (which were not implemented in the simulations presented in this paper). We suspect that this change will be necessary to maintain successional diversity indefinitely in old growth, but we do not expect that gap phase dynamics would substantially affect old growth carbon storage because most trees in old growth belong to shade tolerant species. To check this supposition, we compared runs of the baseline model with identical runs of **H3** – a model in which understory cohorts were drawn at random (independent of size) to fill space in the canopy opened by canopy tree mortality. Comparisons between the three alternative models (**H1**-**H3**) and the baseline model (**H0**) were based on simulations with one species (sugar maple).

2.2.3 Comparison with a standard biogeochemical model

To explore how incorporating individual-level competition and successional diversity into land models affects carbon accumulation in vegetation and soil, we compared the LM3-PPA predictions to those of a CENTURY-like standard biogeochemical (BGC) model (Fig. S1b) as described in Parton et al. (1987) and Luo et al. (1999). Like most current DGVMs and land surface models, the standard BGC model that we implemented was formulated at the level of the grid cell without explicitly scaling from individual plants to ecosystem-level dynamics. In such models, photosynthesis and respiration submodels simulate the net influx of C (NPP) at the level of the grid cell. NPP is then allocated to grid-cell level plant C pools and, after senescence, plant

568 carbon moves through litter and soil pools before returning to the atmosphere. Carbon allocation
569 coefficients and residence times in the various pools determine total carbon storage (Weng and
570 Luo, 2011). We chose this BGC model because all of its C pools – leaves, fine roots, sapwood,
571 heartwood, labile soil carbon, and recalcitrant soil carbon – can be precisely matched to
572 quantities predicted by LM3-PPA. The BGC model simulations were forced with the NPP
573 produced by the single-species runs of LM3-PPA, and so differed only in the patterns of
574 allocation and residence times assumed in the standard BGC model and those that emerged by
575 aggregating finer-scale patterns in LM3-PPA.
576
577 **2.3 Competitive allocation strategies at different CO_2 concentrations**
578 A competitively optimal allocation strategy is the one that can competitively exclude all others.
579 This can be significantly different from the allocation strategy that most effectively uses
580 available resources (i.e., the optimal monoculture strategy). The analytical model derived by
581 Farrior et al. (2013; in revision) predicts that increased leaf-level water use efficiency from CO_2
582 fertilization should cause a shift in the competitively optimal allocation strategy among fine roots,
583 leaves, and wood, which in turn causes the changes in carbon storage described in the Discussion
584 of this paper. We simulated competition among red maple variants with different target fine root
585 biomasses under each of two atmospheric CO_2 concentrations [CO_2] in LM3-PPA: 280 ppm for
586 **preindustrial** and 560 ppm for **doubled** [CO_2]. All runs shared the same meteorological forcing.
587 All red maple variants shared all parameters except for the ratio of fine root to leaf surface area
588 (φ_{RL}) for canopy individuals. Because the target crown LAI of a canopy tree (l_C^*) was constant
589 across red maple variants – and because the amount of carbon allocated to wood depends on the
590 amount of NSC not taken by leaves and fine roots (see Appendix A) – variation in canopy-tree

591 φ_{RL} among variants had little effect on leaf allocation but strong effects on fine-root and wood
592 allocation. Across different monocultures that differ only in φ_{RL}, fine-root allocation should
593 increase and wood allocation should decrease with increasing φ_{RL}, at least in the region of
594 parameter space near the competitive optimum. Note that this fine-root vs. wood allocational
595 tradeoff is not necessarily apparent when comparing allocational types in competition with each
596 other. For example, relatively high φ_{RL} may offer a competitive advantage if trees are water-
597 limited, which could increase carbon gain and fractional wood allocation compared to less
598 competitive types with lower values of φ_{RL} that have little NSC available for wood growth.
599 We performed three sets of experiments with different canopy-tree variants with φ_{RL}
600 ranging from 0.5 to 1.0 (understory φ_{RL} was 0.8 for all variants). Each experiment was performed
601 at both preindustrial and doubled [CO_2] (Table 3):
602 **(1) Polyculture runs** were initiated with five variants (φ_{RL} = 0.5, 0.6, 0.7, 0.8 and 0.9) all having
603 the same initial population density (250 seedlings ha^{-1}). Polyculture runs simulated competition
604 among the five variants for 500 years to identify the most competitive strategy.
605 **(2) Monoculture runs** were performed for each of the five above variants (φ_{RL} = 0.5, 0.6, 0.7,
606 0.8 and 0.9) to identify the most productive strategy in monoculture. Each run simulated the
607 dynamics of a single variant for 500 years.
608 **(3) Invasion runs** were performed for six pairwise combinations of four variants (φ_{RL} = 0.6, 0.7,
609 0.9, and 1.0) (see Table 3 for details of the combinations at the two [CO_2] levels) to confirm the
610 identity of the most competitive strategy identified in the polyculture runs. Each invasion run
611 included two different variants: a "resident" variant and an "invader" variant. We first ran the
612 model with only the resident present for 400 years, which was long enough for it to come close
613 to an equilibrium state. At the beginning of year 401, we converted 5% of the population in each

614 resident cohort into a new invader cohort by changing φ_{RL}. We then ran the model for a further
615 240 years to get the DBH growth rates of invaders. To determine if a $\varphi_{RL} = X$ was an
616 evolutionarily stable strategy (ESS, a strategy that cannot be invaded when in monoculture) we
617 examined runs in which the resident had $\varphi_{RL} = X$ and the invader had $\varphi_{RL} = X \pm \delta$. We also
618 verified that the ESSs at the two CO2 concentrations are convergence stable (Geritz et al., 1998)
619 by examining runs in which the resident had $\varphi_{RL} = X \pm \delta$ (with $\delta = 0.1$ or 0.2) and the invader
620 had $\varphi_{RL} = X$.
621
622 **3 Results**
623 **3.1 GPP, NPP, tree growth rates and abundances**
624 Below, we focus on annual to successional time scales because diurnal and seasonal patterns are
625 caused by the structure of the biophysical parameterizations in LM3-PPA (Appendix A and B),
626 which are identical to those in LM3, have been under development for more than a decade, and
627 are reviewed elsewhere (Shevliakova et al., 2009; Milly et al., 2014). Predicted diurnal and
628 seasonal patterns of GPP, NPP and evapotranspiration by the model are shown in Fig. S2 in
629 Supplemental materials.
630 The model-simulated annual GPP and NPP for the Willow Creek Ameriflux site are close
631 to estimates from eddy covariance and biometric data collected at the same site (Fig. 2a; Desai et
632 al., 2008; Curtis et al., 2002). NPP in the model was 48% of GPP at the approximate steady state.
633 The slight decline of GPP after forest closure was caused by self-thinning (Fig. S3a). Model
634 predictions in Fig. 2 are taken from the monoculture sugar maple runs, but the three-species runs
635 predicted very similar values after the first 20 years (Fig. S4).

636 The allocation of NPP to leaves, fine roots, and woody biomass predicted by LM3-PPA is
637 roughly similar to the measurements in Curtis et al. (2002), with the allocation to wood being too
638 high, and the allocation to leaves and roots too low (Fig. 2b). We did not tune the model to better
639 predict the allocation data at Willow Creek, in part because the difference between the model and
640 data could be caused by the fact that we simulated only one or three of the ~10 species at Willow
641 Creek. Because the allocation scheme assumes that NSC is allocated preferentially to the leaf
642 and fine root targets, interannual variation of sapwood and seed production is greater than that of
643 leaves and fine roots (Fig. 2b).
644 DBH growth rates in the canopy layer are much higher than in the understory (Fig. 2c)
645 because of shading (Fig. S2a in Supplemental materials). The predicted DBH growth rates of
646 upper-canopy trees agree well with those derived from FIA data (Zhang et al., 2014) for all three
647 species (Fig. 3). Predicted understory growth rates for sugar maple also agree well with estimates
648 from FIA data, but predicted understory growth rates for red maple and trembling aspen are
649 lower than estimates from FIA data (Fig. 3).
650 With initial population densities taken from early-successional FIA plots (Table C4), the
651 LM3-PPA model correctly predicts the subsequent successional turnover of trembling aspen, red
652 maple, and sugar maple (compare Fig. 4a and b). The transition from trembling aspen to sugar
653 maple dominance is caused primarily by low survivorship of aspen in the understory, which was
654 due to a combination of growth suppression from shading (which keeps cohorts in small size
655 classes, where understory mortality rates are highest; Fig. 1a) and aspen's relatively high
656 background rate of understory mortality (Table 1 and Eq 8). Mortality due to carbon starvation
657 rarely occurred in our simulations, although this may simply reflect our parameterization of
658 mortality, which attributes high rates of mortality in small size classes to "background mortality"

659 (Fig. 1a), with "starvation mortality" occurring in our model only if NSCs drop to zero. The
660 timing of the transition from aspen to sugar maple is set primarily by the longevity of aspen
661 canopy trees.

662 The model-predicted size distributions of both numbers and biomass for stands at 40-60
663 years and 80-100 years are also qualitatively similar to FIA data (Fig. 5), despite significant
664 quantitative differences in tree numbers. These differences are likely to be caused primarily by a
665 combination of model error, the fact that our simulations included only a subset of species in the
666 FIA plots, and differences between the initial conditions of early successional plots today (which
667 were used to initialize the simulations) and those 40-100 years ago (when succession began in
668 the 40-100 year-old FIA plots).

669 The number of small trees in the baseline LM3-PPA model (**H0**; see Fig. 1 and Table 2)
670 is significantly reduced near the late-successional equilibrium (Fig. 6a; mean model state from
671 600-1000 years). Moreover, the size distribution predicted for these old growth forests has
672 considerable biomass in trees larger than 1.2 m in diameter, which is unrealistic for these species
673 (Fig. 6c). The alternative model **H1** (high mortality rate for large trees) removes the
674 unrealistically large trees. Like H1, cessation of crown area expansion at high DBH (**H2**) reduces
675 the predicted number of very large trees. **H2** also predicts a decline in DBH growth rate as trees
676 become very large (Fig. S6 in Supplemental materials), which is consistent with observations
677 (Sillett et al., 2010; Lorimer et al., 1999). The random selection of understory trees to fill canopy
678 layer gaps (**H3**) has little impact on size and biomass distributions (Fig. 6). GPP and NPP (Fig.
679 S7a), and allocation of NPP to leaves, fine roots, and sapwood (Fig. S7b) simulated with the
680 three alternative assumptions were close to those simulated by the default model (**H0**). The
681 assumption of high mortality rates of very large trees (**H1**) led to reduced woody biomass since

682 this assumption increased the mean turnover rate of wood, but it did not significantly affect
683 equilibrium soil C. Assumptions **H2** and **H3** had little impact on C storage in wood or in the soil
684 (Fig. S7c).
685
686 **3.2 Effects of vegetation dynamics on vegetation and soil C storage**
687 Comparisons of the predictions of LM3-PPA to those of the standard BGC model (Fig. S1b),
688 forced with the same GPP and NPP from LM3-PPA, highlight the effects of successional
689 diversity on carbon storage. The single species runs of LM3-PPA include a dominant species for
690 the region (sugar maple), which is dominant precisely because it is a long-lived late-successional
691 species (Burns and Honkala, 1990). Parameters for the standard BGC model were chosen to be
692 consistent with the one-species LM3-PPA model, and so, as expected, the BGC model and the
693 single-species runs of LM3-PPA predict similar patterns of biomass and soil carbon storage (Fig.
694 7a and b).
695 In contrast, the three-species runs of LM3-PPA are dominated early in succession by a
696 pioneer species (trembling aspen), which is short-lived, perhaps because its low wood density
697 trades resistance to disease and windthrow for rapid height growth (Burns and Honkala, 1990).
698 As a result, three-species runs of LM3-PPA predict lower carbon storage in the woody biomass
699 C pool (Fig. 7a) and higher soil carbon (Fig. 7b) early in succession than the standard BGC
700 model or the single-species runs of LM3-PPA. The woody biomass C pool with one species
701 needs ~300 years to reach equilibrium, whereas the three-species runs needed more than 500
702 years (Fig. 7a).
703 In the standard BGC model, the turnover rate of the woody biomass carbon pool was set
704 as the mean mortality rate of sugar maple trees in the canopy layer (0.012 yr^{-1}). In contrast, in the

LM3-PPA simulation with one species, there was a peak in the biomass turnover rate because of the self-thinning of trees that had been pushed into the understory after canopy closure (red dashed line in Fig. 7c). In the LM3-PPA simulation with three species, the biomass turnover rates were much higher early in succession than in the single-species run because the mortality rates of aspen, and to a lesser extent red maple, are higher than that of sugar maple (green dashed line in Fig. 7c). The peak in the biomass turnover rate in the three-species run early in succession is caused by self-thinning following canopy closure, which occurs at a younger stand age than in the single-species run. As the models approached their equilibrium states, the carbon in biomass and soil pools converged because the inputs (NPP) and the residence times in biomass and soil C pools converged (Fig. 7).

3.3 Competitively optimal allocation strategy at different atmospheric CO_2 levels

After 500 years of competition among five allocation strategies of red maple (with the ratio of crown LAI to fine root area, φ_{RL}, ranging from 0.5 to 0.9 for upper-canopy trees) in the "polyculture runs", the variant with φ_{RL}=0.7 had the highest basal area at preindustrial [CO_2] (280 ppm), whereas φ_{RL}=0.9 had the highest basal area at doubled [CO_2] (560 ppm) (Fig. 8). These results suggest that φ_{RL}=0.7 and φ_{RL}=0.9 are approximate competitive optima at 280 ppm and 560 ppm, respectively. The precision of the approximations is limited by the resolution of the experiments (five discrete values of φ_{RL}).

These approximate competitive optima were confirmed to be approximate ESSs by two-species "invasion runs" in which an equilibrium monoculture of one variant (a species with a given value of φ_{RL}) competed against an invading alternative variant (a species with a different value of φ_{RL}) that was initially rare. At [CO_2] = 280 ppm, φ_{RL}=0.7 was the competitively optimal

728 strategy since it could not be invaded by any other variant and could invade all other variants
729 (i.e., the convergence-stable ESS; Geritz et al., 1998); and at [CO_2] = 560 ppm φ_{RL}=0.9 was the
730 competitively optimal strategy (Fig. 9).
731 Using the results in Farrior et al. (2013; in revision), it is possible to show mathematically
732 that − for the case considered here, where understory traits are constant across species/PFTs – the
733 competitive optimum (ESS) reduces to the strategy with the highest woody NPP when in the
734 canopy and when in competition with the other strategies. Note also, that species rankings of
735 lifetime reproductive success, woody NPP, and DBH growth rate are equivalent here because all
736 variants share the same other vital rates, wood density, and stem allometry. In the polyculture
737 simulations, the strategy with the highest woody NPP or DBH growth rate in the canopy (over
738 the last 60 simulation years) was φ_{RL}=0.7 at preindustrial [CO_2], and φ_{RL}=0.9 at doubled [CO_2]
739 (Fig. 10), which further confirms the CO_2-induced allocational shift implied by the results
740 described above. The mechanisms causing this allocational shift under elevated [CO_2] are
741 explored in detail in the Discussion. Here, we simply note that these results imply that woody
742 carbon sinks caused by elevated [CO_2] will be reduced by competitively optimal shifts in
743 allocation away from long-lived woody tissues and toward short-lived fine roots, either because
744 of an evolved plastic response or because a species or genotype with a larger φ_{RL} will become
745 competitively dominant under elevated [CO_2] (Farrior et al., 2013).
746 In contrast, among the "monoculture runs", the strategies with the highest canopy woody
747 NPP and DBH growth rates were φ_{RL}=0.6 and φ_{RL}=0.7 for preindustrial and doubled [CO_2],
748 respectively (Fig. 10). Both of these monoculture optima have higher allocation to wood and less
749 allocation to fine roots than monocultures of the corresponding competitive optima (φ_{RL}=0.7 and
750 φ_{RL}=0.9 at preindustrial and doubled [CO_2], respectively). Note that in Fig. 10, competitively

751 optimal growth rates are sometimes higher than those for the monoculture optima. This is
752 because the competitively optimal growth rates in Fig. 10 are from polyculture runs, where
753 individuals of the most competitive strategy have access to more water than in a monoculture of
754 their own strategy; i.e., in polyculture, individuals of the most competitive strategy compete
755 against individuals whose fine-root density is lower than that of the most competitive strategy.
756 To understand how differences between the monoculture and competitive optima arise,
757 consider the following example. Under preindustrial [CO_2], φ_{RL}=0.7 had higher DBH growth rate
758 than φ_{RL}=0.6 when invading a monoculture in which light and water availabilities were
759 determined primarily by φ_{RL}=0.6. For this reason, the model predicts that φ_{RL}=0.7 will
760 competitively exclude φ_{RL}=0.6, even though it will have a lower equilibrium growth rate once it
761 has taken over the stand (because φ_{RL}=0.7 has a lower growth rate in conditions created by
762 φ_{RL}=0.7 than φ_{RL}=0.6 has in conditions created by φ_{RL}=0.6). These differences between the
763 competitive (polyculture) and non-competitive (monoculture) optima illustrate that plant
764 strategies predicted by naïve (e.g., productivity-maximizing) optimization algorithms are often at
765 odds with predictions from game-theoretic (ESS) competitive optimization (McNickle and
766 Dybzinski, 2013; Farrior 2014).
767 Fig. 11 contains additional results that will be used in the Discussion to explain the
768 predicted allocational shift caused by elevated [CO_2]. It reports the percentage difference
769 between two runs of a monoculture of φ_{RL}=0.7 at [CO_2]=560ppm and at preindustrial [CO_2] for
770 each of five quantities. A doubling of [CO_2] increased the fraction of each growing season in
771 which canopy trees were water-saturated (defined as the fraction of days during the growing
772 season in which water supply was greater than or equal to demand at 2:00 p.m. over the final 60
773 years of a 500-year run) by 21%. The water use efficiency (WUE; GPP per unit transpiration) of

canopy trees during the water-limited period (days in which water supply was less than demand at 2:00 p.m.) increased by 79%. The change in the length of the water-saturated period is relatively small (21% increase, compared to a 79% increase in WUE during the water-limited period) because of biophysical feedbacks in the model. Specifically, although a doubling of [CO_2] decreased transpiration by 4.55% for the whole tile, this change was offset by a 1.78% increase in the sum of evaporation and runoff. In absolute terms, the decrease in transpiration was 10.1 mm/yr, while the increase in evaporation plus runoff was 10.2 mm/year, which canceled the effect of increased [CO_2] on mean growing-season soil moisture (152.49 mm at preindustrial [CO_2] and 152.91 mm at doubled [CO_2]).

4 Discussion

4.1 Overview

In this paper, we describe the biophysical coupling between the height-structured PPA forest dynamics model and the GFDL LM3 land model. The new model, LM3-PPA, was developed for future Earth system model (ESM) simulations in which vegetation dynamics are based on individual-level resource competition among size-structured cohorts of plants belonging to multiple species or PFTs. Our paper describes (1) the details of the biophysical coupling between LM3 and PPA, (2) preliminary model evaluation for a single site in the northeastern USA, (3) simulation experiments involving multiple allocational types at different atmospheric CO_2 concentrations, and (4) an interpretation of these competition experiments based on a mathematically tractable version of the PPA model. LM3-PPA is among the first land models to represent individual-level resource competition − including height-structured competition for light – and is the only land model to date that is closely tied to a mathematically tractable forest

797 dynamics model, which affords a greater level of understanding of land model behavior than
798 would be possible otherwise. Our paper is novel because we present novel land-model
799 predictions of how resource competition affects allocation to wood (a long-lived C pool) vs. fine
800 roots (a short-lived C pool) at different CO_2 levels, and because we show how these land-model
801 predictions can be understood in the context of analytical predictions derived from a
802 mathematically tractable version of the PPA model, as explained in Section 4.5 below.
803
804 **4.2 Model evaluation**
805 The comparisons between the model's predictions and data at various scales (Figs. 2-5, and Fig.
806 S5 in Supplemental materials) are intended as an initial evaluation and validation of LM3-PPA.
807 The comparisons show that the model produces reasonable fast time-scale carbon and water
808 dynamics (Supplemental materials) as well as reasonable annual values for GPP and NPP (Fig.
809 2). The model also makes realistic predictions of individual growth rates, population structure
810 (Fig. 5), and forest succession (Fig. 4). These comparisons must be evaluated in light of the
811 tuning of the physiological model to produce observed NPP, the tuning of a single parameter
812 affecting diameter growth, and the tuning of the elevated mortality of seedlings and small
813 saplings.
814 The model formulation predicts tree- and ecosystem-level allocation patterns that are
815 supported by a number of empirical studies. In LM3-PPA, the ratio of NPP to GPP and the
816 fraction of NPP allocated to the three main plant structural C pools (foliate, fine roots, and wood)
817 are not assumed to directly depend on tree size and stand age. Nonetheless, foliage and fine root
818 biomasses equilibrate in the model more than an order of magnitude more quickly than woody
819 biomass. Experimental studies have indeed found that leaves and fine roots reach equilibrium

820 quickly, long before total biomass reaches equilibrium (Goulden et al., 2011). Studies have also
821 found that the ratio of autotrophic respiration to GPP is independent of age (Ryan et al., 2004),
822 which is consistent with our model. Note that this is contrary to the expectation that maintenance
823 respiration of stems should increase with tree size if it is proportional to sapwood biomass.
824 Instead, LM3-PPA assumes that stem maintenance respiration is proportional to crown area,
825 which – like fine root surface area – is assumed to be proportional to $DBH^{1.5}$ (see Dybzinski et
826 al., 2011; Farrior et al., 2013). This is consistent with the finding that bole respiration per unit of
827 biomass decreases with age (Ryan et al., 2004). Also, it is possible to show that if NPP and
828 crown area are proportional to $DBH^{1.5}$, and both DBH growth rate and fractional allocation of
829 NPP to wood are size-independent, then wood biomass should be proportional to $DBH^{2.5}$, as it is
830 in the model and in empirical reports (e.g., Jenkins et al., 2003; Wang, 2006).
831 Because LM3-PPA is based on macroscopic equations from gap simulators (Strigul et al.,
832 2008), forest inventory data can also be used to evaluate the model. LM3-PPA was tuned to
833 reproduce canopy tree growth rates for three tree species near Willow Creek, but was not tuned
834 to fit understory growth rates, which therefore provide useful tests of model performance.
835 Observed understory growth rates for the two least shade-tolerant species were under-predicted
836 (Fig. 3; note that uncertainties in mean growth rates are much smaller than the variances in the
837 growth observations shown by the error bars in Fig. 3). One likely reason for this model-data
838 discrepancy is that shade intolerant species such as trembling aspen tend to experience darker
839 understory conditions in our simulations (which assume homogeneous light conditions within
840 each understory layer) than in real forests, where saplings of shade intolerant species tend to
841 occur in unusually bright understory locations (Lichstein et al., 2010; Davies, 2001; Clark and
842 Clark, 1992; Poorter and Arets, 2003).

LM3-PPA also predicts the observed successional turnover of trembling aspen, red maple and sugar maple and size structure in the forests of the northern Lake States, USA (Figs 4 and 5; see also Woods, 2000; Purves et al., 2008). The model's ability to make detailed 100-year predictions that are consistent with data from successional chronosequences is not surprising because forest simulators have been succeeding in this type of prediction for decades. However, it does reaffirm the value of constructing a DGVM from the scaling algorithms in forest gap simulators.

Although LM3-PPA successfully captures the main features of secondary forest succession in the northern Lake States, USA (as does the PPA model; Purves et al. 2008), we would not expect LM3-PPA to maintain successional diversity indefinitely in old-growth forests. This is because LM3-PPA (like the PPA model) does not represent the gap-scale disturbances that shade-intolerant species require for persistence in old-growth. Future implementations of LM3-PPA may include the gap-dynamics approximation from the ED model (Moorcroft et al., 2001), which should allow successional diversity to be maintained in old-growth, and which may also capture other forms of spatial heterogeneity (e.g., the presence of emergent trees in some tropical forests). As explained in Section 5 of Appendix A, the ED gap-age approximation is already built into the LM3-PPA model code (but was not used in the simulations presented here).

4.3 Alternative assumptions about effects of size and age on growth and mortality.

In the baseline LM3-PPA model (H0 in Table 2), canopy tree mortality rates are constant and independent of tree size and age, and canopy tree diameter growth rates remain roughly constant after approaching an asymptote when trees are still small (see text below Eq. 17). As a result, the model predicts unrealistically large trees in old forests (Fig. 6). Although this is a common

problem of forest simulators, it is often not very important in regions of the world where little old-growth remains (e.g., the temperate zone) or where stand-replacing natural disturbances are relatively common (e.g., fire-prone boreal forests). We explored alternative assumptions about growth and death rates of very large trees in this paper, primarily because LM3-PPA will ultimately need to perform in regions, such as the wet tropics, where old growth forests are more common. Of the hypotheses examined (H0-H3), size-dependent decrease in the exponent relating crown area and diameter (H2) provides the best mix of empirical support and ability to produce realistic size distributions. Note, however, that none of the alternative assumptions about large trees has a large effect on predicted ecosystem-level carbon fluxes or storage in 600-1000 year-old forests that are at quasi-equilibrium (Fig. S7).

4.4 Effects of vegetation structure and successional diversity on C dynamics

For the tests that we have applied to date, the extra structure and diversity in LM3-PPA has relatively little effect on diurnal patterns of fluxes or annual NPP and GPP, but does affect long-term carbon accumulation. The successional effects of size structure are best seen in the three-species run in Fig. 7c (green dashed line), where the biomass turnover rate first climbs by ~30% and then falls by more than a factor of 3 over the first 200 years of succession because of the successional transition from aspen, which has a high mortality rate, to sugar maple, which has a low mortality rate. As a result, carbon accumulation in the three-species run of LM3-PPA is significantly lower than that in the single-species run for more than 200 years (Fig. 7a).

The woody carbon accumulation rate after *t* years of succession in a simple biogeochemical box model is approximately $\alpha_w NPP \cdot \mathrm{e}^{-\mu t}$ (where α_w is the fraction of NPP allocated to wood and μ is the annual tree mortality rate) (Weng et al., 2012). Thus, the biomass

889 growth rate in the standard BGC model exponentially decays over time to yield the asymptotic
890 biomass accumulation curve in Fig. 7a (solid line). In contrast, in the PPA, an even-aged cohort
891 of shade-intolerant saplings will self-thin so that the sum of their crown areas equals the area of
892 the disturbance they are competing to fill. That is, the number of individuals in the cohort, $n(t)$,
893 tends to be proportional to the reciprocal of an individual's crown area, $A_{CR}(D(t))$. Since total
894 biomass is simply individual biomass, $b(D(t))$, multiplied by $n(t)$, total stem biomass tends to be
895 proportional to $b(D(t))/A_{CR}(D(t))$, which − given the allometric constants for wood biomass,
896 $S(D(t))$, and $A_{CR}(D(t))$ − is simply proportional to diameter, $D(t)$ (see Eq. 4). Finally, because
897 diameter grows at an approximately constant rate after saplings reach ~10 cm in diameter
898 (around year 30 in Fig. 2c), LM3-PPA predicts linear biomass growth for an extended period
899 when shade intolerant species are present, like the green dashed line in Fig. 7a, and as observed
900 in real chronosequences (Yang et al., 2011) .
901
902 **4.5 Competitive optimization and ecosystem C storage**
903 When [CO_2] doubles from 280 to 560 ppm, the most competitive strategy in LM3-PPA shifts
904 toward trees with greater allocation to fine roots and less allocation to wood (Figs. 8-10). This is
905 important because it would reduce the carbon sink caused by CO_2 fertilization. Thus, competitive
906 optimization provides a way to discover carbon cycle feedbacks that involve changes in
907 ecosystem-level allocation.
908 Elevated [CO_2] leads to greater leaf-level or intrinsic water use-efficiency (WUE; carbon
909 fixation per unit transpiration) in LM3-PPA, as observed in CO_2 enrichment experiments (Norby
910 and Zak, 2011). Higher leaf-level WUE in LM3-PPA increases leaf productivity during the
911 water-limited period of the growing season, while also decreasing the proportion of the growing

912 season that plants spend in water limitation. These two responses to increased [CO_2] have
913 opposing effects on the most competitive fine-root allocation strategy (i.e., the evolutionarily
914 stable strategy, ESS; Farrior et al., 2013; Farrior et al., in revision). ESS root allocation increases
915 with increasing productivity (due to high water availability or high water use efficiency) during
916 the water-limited period (up until the point where plants are water-saturated, and thus no longer
917 water-limited) for competitive reasons related to "the tragedy of the commons" for water use in
918 plants (Gersani et al., 2001; Zea-Cabrera et al., 2006; Farrior et al., 2013). In contrast, ESS root
919 allocation decreases as the length of the water-saturated period increases because roots represent
920 a respiratory sink when plants are water saturated. The net effect of an increase in [CO_2] on the
921 ESS depends on the quantitative balance between these two opposing forces (Farrior et al., in
922 revision), and thus depends on the full suite of biophysical feedbacks present in a model like
923 LM3-PPA that must exchange matter, energy and momentum with the atmosphere. In the case
924 study presented here, increased evaporation and runoff largely compensate for reduced
925 transpiration under elevated [CO_2], so that [CO_2] has little effect on mean soil moisture or the
926 total number of hours each growing season during which plants are water saturated (Fig. 11). In
927 contrast, increased evaporation and runoff under elevated [CO_2] do not attenuate the expected
928 increase in leaf productivity (due to increased WUE) during the period when water is limiting.
929 The upshot, in our case study, is that of the two opposing forces on ESS fine-root allocation – (1)
930 a decrease in root allocation due to an increased period of water-saturation, vs. (2) an increase in
931 root allocation due to increased leaf productivity during the water-limited period − the latter
932 effect dominates, and the most competitive strategy shifts to one with greater allocation to fine
933 roots (Figs. 8-10). This result has now focused our attention on the strength of the biophysical
934 feedbacks in LM3 and LM3-PPA, which might be too strong. The important point here is that we

know what to focus on only because of the understanding afforded by the connection between LM3-PPA and the analytically tractable PPA model (Farrior et al., 2013; Farrior et al., in revision). We understand the predicted feedback in LM3-PPA involving [CO_2], water, fine-root allocation and carbon storage only because the model may be interrogated analytically.

4.6 Future challenges

In this paper, we do not provide parameter values needed to implement LM3-PPA at the global scale using PFTs or more flexible trait-based approaches (e.g., Scheiter et al., 2013; Wullschleger et al., 2014). The PPA has previously been applied to other temperate forest types that include conifers (e.g., Purves et al., 2008; Strigul et al., 2008), as well as tropical forests with more than two canopy layers (Bohlman and Pacala, 2012); and we are currently developing parameter values for non-tree vegetation types, such as shrubs and grasses (Weng et al., unpublished). The formalism we describe in this paper requires no structural changes to work in non-forested ecosystems, including those with open canopies or with no competition for light (i.e., because of severe water limitation). Furthermore, as explained in Appendix A, the current version of the LM3-PPA code can already accommodate land use change, secondary forest management, stand-replacing disturbance, and the ED approximation for canopy gap dynamics, which is required to maintain successional diversity in old growth forests with low rates of stand-replacing disturbance. In summary, LM3-PPA can, in principle, be extended to global-scale simulations in fully-coupled ESM experiments with little modification to the processes already encoded in the model.

In addition to developing parameterizations for global-scale applications, another important area for future work is to better understand the transient dynamics of vegetation

response to global change. Our results suggest potentially important effects of allocational shifts, driven by competition among plants for light and water under elevated CO_2, on terrestrial carbon balance. However, our competition experiments were designed only to identify the eventual outcome of competition under a given set of conditions, and are therefore agnostic about the rate and pathway of response. In reality, allocational shifts could be potentially rapid (e.g., tracking environmental conditions on an annual time scale) if individual plasticity were sufficient (Franklin et al., 2012), would occur over intermediate time scales (e.g., decadal) if allocational shifts required shifts in relative abundances of species already present within a landscape, and would be even slower if allocational shifts required long-distance migration by dispersal-limited species (Lischke et al., 2006; Snell et al., 2014) and/or the evolution of novel types (Valladares et al., 2007). Empirical evidence suggests that intraspecific variation in allocation is often sufficient to accommodate the shift in competitively optimal allocation predicted by LM3-PPA under a doubling of atmospheric CO_2 (R. Dybzinski, unpublished analysis), and Free-air CO_2 Enrichment (FACE) experiments demonstrate considerable individual plasticity in allocation to leaves, wood, and fine roots (Jackson et al., 2009; McCarthy et al., 2010; Norby and Zak, 2011; Iversen et al., 2012). However, there are clearly limits to plasticity (Valladares et al., 2007), and it is unknown if the plastic responses of individuals to environmental change (which evolved over the last ~20 million years under relatively low atmospheric CO_2 concentrations; Zachos et al., 2001) would be the competitively optimal responses under future novel conditions. A key challenge, then, is to better understand the transient dynamics that ecosystems will undergo as they approach competitive equilibria from different initial conditions.

5 Conclusions

We present a model, LM3-PPA, which simulates vegetation dynamics and biogeochemical processes by explicitly scaling from individual plants to ecosystems using the Perfect Plasticity Approximation (PPA). The model is formulated to be the land surface component of an Earth System Model. It includes height-structured competition for light and root allocation-dependent competition for below-ground resources (water in this study). The partitioning of space by plant crowns following the rules of the PPA to form canopy layers simplifies the simulation of light competition among trees and allows the LM3-PPA model to predict forest succession with an explicit description of the size distributions of individuals within each species or functional type, in addition to the predictions of carbon fluxes of an ecosystem (GPP, NPP, and R_a), the dynamics of soil organic matter and decomposition (heterotrophic respiration, R_h), evapotranspiration, and soil hydrology. Because of the tractability of the PPA, the coupled LM3-PPA model is computationally efficient (relative to existing alternatives to modeling height-structured, individual-level competition within ESMs) and retains close linkages to mathematically tractable special cases (e.g., constant climate).

Comparisons of model simulations with data show that the model makes reasonable predictions for diurnal and annual carbon and water fluxes, growth rates of individual trees, and population sizes and species turnover during succession. The model marginally under-predicts the growth rates of shade intolerant species in the understory and seriously over-predicts of abundances of very large trees in old growth. The overestimate of large trees can be corrected by adding either size specific mortality or size specific crown area allometry, both of which are supported by some studies. The model also shows that within-functional-type successional diversity has significant ecosystem-level effects at time scales up to a century or more. Finally,

simulation experiments show that the dominant competitor's root-leaf-stem allocation pattern shifts as a function of the atmospheric CO_2 concentration and predict that carbon sinks caused by CO_2 fertilization in forests limited by light and water will be down-regulated if allocation tracks changes in the competitive optimum. These results indicate that the ecological strategies functioning at the scales of individuals and communities, which are usually missing in ESMs, have strong impacts on biogeochemical processes and their responses to climate changes.

The implementation of the model in this paper is for temperate broadleaved forest trees, but the formulation of the model is general and can be expanded to include other growth forms and physiologies. The model can accommodate an arbitrary number of functional types, species and/or genotypes in competition with one another across the terrestrial regions of the globe.

Acknowledgements

Funding was provided by the USDA Forest Service Northern Research Station (agreements 09-JV-11242306-051, 13-JV-11242315-066, and 11-JV-11242306-059) and the Princeton Environment Institute. We thank Catherine Raphael of the Geophysical Fluid Dynamics Laboratory for drawing the Fig. S1a, and Drs. Richard Birdsey and Yude Pan of the USDA Forest Service for helpful comments on an earlier version of this paper. We thank Drs. Takashi Kohyama, Rosie Fisher, Benjamin Poulter, and Matthew Smith for careful and thoughtful reviews that greatly improved the clarity of the paper.

References

Bohlman, S., and Pacala, S.: A forest structure model that determines crown layers and partitions growth and mortality rates for landscape-scale applications of tropical forests, J. Ecol., 100, 508-518, doi:10.1111/j.1365-2745.2011.01935.x, 2012.

Bonan, G. B.: Forests and climate change: Forcings, feedbacks, and the climate benefits of forests, Science, 320, 1444-1449, doi:10.1126/science.1155121, 2008.

Botkin, D. B., Wallis, J. R., and Janak, J. F.: Some Ecological Consequences of a Computer Model of Forest Growth, J. Ecol., 60, 849-872, doi:10.2307/2258570, 1972.

Chapin, F. S., Randerson, J. T., McGuire, A. D., Foley, J. A., and Field, C. B.: Changing feedbacks in the climate-biosphere system, Front. Ecol. Environ., 6, 313-320, doi:10.1890/080005, 2008.

Clark, D. A., and Clark, D. B.: Life-History Diversity of Canopy and Emergent Trees in a Neotropical Rain-Forest, Ecol. Monogr., 62, 315-344, doi: 10.2307/2937114, 1992.

Coates, K. D., Canham, C. D., Beaudet, M., Sachs, D. L., and Messier, C.: Use of a spatially explicit individual-tree model (SORTIE/BC) to explore the implications of patchiness in structurally complex forests, For. Ecol. Manage., 186, 297-310, doi:10.1016/S0378-1127(03)00301-3, 2003.

Curtis, P. S., Hanson, P. J., Bolstad, P., Barford, C., Randolph, J. C., Schmid, H. P., and Wilson, K. B.: Biometric and eddy-covariance based estimates of annual carbon storage in five eastern North American deciduous forests, Agr. Forest Meteorol., 113, 3-19, 2002.

Davies, S. J.: Tree mortality and growth in 11 sympatric Macaranga species in Borneo, Ecology, 82, 920-932, 2001.

Desai, A. R., Noormets, A., Bolstad, P. V., Chen, J. Q., Cook, B. D., Davis, K. J., Euskirchen, E. S., Gough, C. M., Martin, J. G., Ricciuto, D. M., Schmid, H. P., Tang, J. W., and Wang, W. G.: Influence of vegetation and seasonal forcing on carbon dioxide fluxes across the Upper Midwest, USA: Implications for regional scaling, Agr. Forest Meteorol., 148, 288-308, doi: 10.1016/j.agrformet.2007.08.001, 2008.

Dunne, J. P., John, J. G., Adcroft, A. J., Griffies, S. M., Hallberg, R. W., Shevliakova, E., Stouffer, R. J., Cooke, W., Dunne, K. A., Harrison, M. J., Krasting, J. P., Malyshev, S. L., Milly, P. C. D., Phillipps, P. J., Sentman, L. T., Samuels, B. L., Spelman, M. J., Winton, M., Wittenberg, A. T., and Zadeh, N.: GFDL's ESM2 Global Coupled Climate-Carbon Earth System Models. Part I: Physical Formulation and Baseline Simulation Characteristics, J. Climate, 25, 6646-6665, doi: 10.1175/Jcli-D-11-00560.1, 2012.

Dunne, J. P., John, J. G., Shevliakova, E., Stouffer, R. J., Krasting, J. P., Malyshev, S. L., Milly, P. C. D., Sentman, L. T., Adcroft, A. J., Cooke, W., Dunne, K. A., Griffies, S. M., Hallberg, R. W., Harrison, M. J., Levy, H., Wittenberg, A. T., Phillips, P. J., and Zadeh, N.: GFDL's ESM2 Global Coupled Climate-Carbon Earth System Models. Part II: Carbon System Formulation and

1060 Baseline Simulation Characteristics, J. Climate, 26, 2247-2267, doi:10.1175/Jcli-D-12-00150.1,
1061 2013.

1062 Dybzinski, R., Farrior, C., Wolf, A., Reich, P. B., and Pacala, S. W.: Evolutionarily Stable
1063 Strategy Carbon Allocation to Foliage, Wood, and Fine Roots in Trees Competing for Light and
1064 Nitrogen: An Analytically Tractable, Individual-Based Model and Quantitative Comparisons to
1065 Data, Am. Nat., 177, 153-166, doi 10.1086/657992, 2011.

1066 Dybzinski, R., Farrior, C. E., Ollinger, S., and Pacala, S. W.: Interspecific vs intraspecific
1067 patterns in leaf nitrogen of forest trees across nitrogen availability gradients, New Phytol., 200,
1068 112-121, doi: 10.1111/Nph.12353, 2013.

1069 Farrior, C. E., Dybzinski, R., Levin, S. A., and Pacala, S. W.: Competition for water and light in
1070 closed-canopy forests: a tractable model of carbon allocation with implications for carbon sinks,
1071 Am. Nat., 181, 314-330, doi:10.1086/669153, 2013.

1072 Farrior, C. E.: Competitive optimization models, attempting to understand the diversity of life.
1073 New Phytol., 203, 1025-2027, doi: 10.1111/nph.12940, 2014.

1074 Farrior, C. E., Rodriguez-Iturbe, I., Dybzinski, R., Levin, S. A., and Pacala, S. W.: Decreased
1075 water limitation under elevated CO_2 amplifies potential for forest carbon sinks, P. Natl. Acad. Sci.
1076 USA, In revision.

1077 Fisher, R., McDowell, N., Purves, D., Moorcroft, P., Sitch, S., Cox, P., Huntingford, C., Meir, P.,
1078 and Woodward, F. I.: Assessing uncertainties in a second-generation dynamic vegetation model
1079 caused by ecological scale limitations, New Phytol., 187, 666-681, doi:10.1111/j.1469-
1080 8137.2010.03340.x, 2010.

1081 Foley, J. A., Prentice, I. C., Ramankutty, N., Levis, S., Pollard, D., Sitch, S., and Haxeltine, A.:
1082 An integrated biosphere model of land surface processes, terrestrial carbon balance, and
1083 vegetation dynamics, Global Biogeochem. Cy., 10, 603-628, doi:10.1029/96gb02692, 1996.

1084 Franklin, O., Johansson, J. , Dewar, R. C. , Dieckmann, U., McMurtrie, R. E., Brannstrom, A.,
1085 and Dybzinski, R.: Modeling carbon allocation in trees: a search for principles. Tree Physiol., 32,
1086 648–666, 2012.

1087 Friedlingstein, P., Cox, P., Betts, R., Bopp, L., Von Bloh, W., Brovkin, V., Cadule, P., Doney, S.,
1088 Eby, M., Fung, I., Bala, G., John, J., Jones, C., Joos, F., Kato, T., Kawamiya, M., Knorr, W.,
1089 Lindsay, K., Matthews, H. D., Raddatz, T., Rayner, P., Reick, C., Roeckner, E., Schnitzler, K. G.,
1090 Schnur, R., Strassmann, K., Weaver, A. J., Yoshikawa, C., and Zeng, N.: Climate-carbon cycle
1091 feedback analysis: Results from the C(4)MIP model intercomparison, J. Climate, 19, 3337-3353,
1092 2006.

1093 Friedlingstein, P., Meinshausen, M., Arora, V. K., Jones, C. D., Anav, A., Liddicoat, S. K., and
1094 Knutti, R.: Uncertainties in CMIP5 Climate Projections due to Carbon Cycle Feedbacks, J.
1095 Climate, 27, 511-526, doi:10.1175/Jcli-D-12-00579.1, 2014.

Friend, A. D., Schugart, H. H., and Running, S. W.: A Physiology-Based Gap Model of Forest Dynamics, Ecology, 74, 792-797, doi:10.2307/1940806, 1993.

Friend, A. D., Stevens, A. K., Knox, R. G., and Cannell, M. G. R.: A process-based, terrestrial biosphere model of ecosystem dynamics (Hybrid v3.0), Ecol. Model., 95, 249-287, doi:10.1016/S0304-3800(96)00034-8, 1997.

Gerber, S., Hedin, L. O., Oppenheimer, M., Pacala, S. W., and Shevliakova, E.: Nitrogen cycling and feedbacks in a global dynamic land model, Global Biogeochem. Cy., 24, GB1001, doi:10.1029/2008gb003336, 2010.

Geritz, S. A. H., Kisdi, E., Meszena, G., and Metz, J. A. J.: Evolutionarily singular strategies and the adaptive growth and branching of the evolutionary tree, Evol. Ecol. 12, 35-57, doi: 10.1023/A:1006554906681, 1998.Gersani, M., Brown, J. S., O'Brien, E. E., Maina, G. M., and Abramsky, Z.: Tragedy of the commons as a result of root competition, J. Ecol., 89, 660-669, doi:10.1046/j.0022-0477.2001.00609.x, 2001.

Goulden, M. L., McMillan, A. M. S., Winston, G. C., Rocha, A. V., Manies, K. L., Harden, J. W., and Bond-Lamberty, B. P.: Patterns of NPP, GPP, respiration, and NEP during boreal forest succession, Global Change Biol., 17, 855-871, doi:10.1111/j.1365-2486.2010.02274.x, 2011.

Haverd, V., Smith, B., Nieradzik, L. P., and Briggs, P. R.: A stand-alone tree demography and landscape structure module for Earth system models: integration with inventory data from temperate and boreal forests, Biogeosciences, 11, 4039-4055, doi:10.5194/bg-11-4039-2014, 2014.

Hruska, J., Cermak, J., and Sustek, S.: Mapping tree root systems with ground-penetrating radar, Tree Physiol., 19, 125-130, 1999.

Iversen, C. M., Keller, J. K., Garten, C. T., and Norby, R. J.; Soil carbon and nitrogen cycling and storage throughout the soil profile in a sweetgum plantation after 11 years of CO_2-enrichment, Global Change Biol., 18, 1684-1697, 2012.

Jackson, R. B., Cook, C. W., Pippen, J. S., Palmer, S. M.: Increased belowground biomass and soil CO2 fluxes after a decade of carbon dioxide enrichment in a warm-temperate forest, Ecology, 90, 3352-3366, 2009.

Jenkins, J. C., Chojnacky, D. C., Heath, L. S., and Birdsey, R. A.: National-scale biomass estimators for United States tree species, For. Sci., 49, 12-35, 2003.

Lichstein, J. W., Dushoff, J., Ogle, K., Chen, A. P., Purves, D. W., Caspersen, J. P., and Pacala, S. W.: Unlocking the forest inventory data: relating individual tree performance to unmeasured environmental factors, Ecol. Appl., 20, 684-699, 2010.

Lischke, H., Zimmermann, N. E., Bolliger, J., Rickebusch, S., and Loeffler, T. J.: TreeMig: A forest-landscape model for simulating spatio-temporal patterns from stand to landscape scale, Ecol. Modelling 199, 409–420, 2006.

Lorimer, C. G., Dahir, S. E., and Singer, M. T.: Frequency of partial and missing rings in Acer saccharum in relation to canopy position and growth rate, Plant Ecol., 143, 189-202, doi: 10.1023/A:1009847819158, 1999.

Luo, Y. Q., Luan, J. S., and Reynolds, J. F.: Responses of a loblolly pine ecosystem to CO2 enrichment: a modeling analysis, Tree Physiol., 19, 279-287, 1999.

Luo, Y. Q., White, L. W., Canadell, J. G., DeLucia, E. H., Ellsworth, D. S., Finzi, A. C., Lichter, J., and Schlesinger, W. H.: Sustainability of terrestrial carbon sequestration: A case study in Duke Forest with inversion approach, Global Biogeochem. Cy., 17, 1021, doi: 10.1029/2002gb001923, 2003.

Luyssaert, S., Inglima, I., Jung, M., Richardson, A. D., Reichsteins, M., Papale, D., Piao, S. L., Schulzes, E. D., Wingate, L., Matteucci, G., Aragao, L., Aubinet, M., Beers, C., Bernhoffer, C., Black, K. G., Bonal, D., Bonnefond, J. M., Chambers, J., Ciais, P., Cook, B., Davis, K. J., Dolman, A. J., Gielen, B., Goulden, M., Grace, J., Granier, A., Grelle, A., Griffis, T., Grunwald, T., Guidolotti, G., Hanson, P. J., Harding, R., Hollinger, D. Y., Hutyra, L. R., Kolar, P., Kruijt, B., Kutsch, W., Lagergren, F., Laurila, T., Law, B. E., Le Maire, G., Lindroth, A., Loustau, D., Malhi, Y., Mateus, J., Migliavacca, M., Misson, L., Montagnani, L., Moncrieff, J., Moors, E., Munger, J. W., Nikinmaa, E., Ollinger, S. V., Pita, G., Rebmann, C., Roupsard, O., Saigusa, N., Sanz, M. J., Seufert, G., Sierra, C., Smith, M. L., Tang, J., Valentini, R., Vesala, T., and Janssens, I. A.: CO2 balance of boreal, temperate, and tropical forests derived from a global database, Global Change Biol., 13, 2509-2537, doi:10.1111/j.1365-2486.2007.01439.x, 2007.

McNickle, G. G., and Dybzinski, R.: Game theory and plant ecology, Ecol. Lett., 16, 545-555, doi:10.1111/Ele.12071, 2013.

Mccarthy, H. R., Oren, R., Johnsen, K. H., Gallet-Budynek, A., Pritchard, S. G., Cook, C. W., LaDeau, S. L., Jackson, R. B., and Finzi, A. C.: Re-assessment of plant carbon dynamics at the Duke free-air CO2 enrichment site: interactions of atmospheric [CO2] with nitrogen and water availability over stand development. New Phytol., 185, 514-528, 2010.

Medvigy, D., Wofsy,S. C., Munger, J. W., Hollinger, D. Y., and Moorcroft, P. R.: Mechanistic scaling of ecosystemfunction and dynamics in space and time: Ecosystem Demography model version 2, J. Geophys. Res., 114, G01002,doi:10.1029/2008JG000812, 2009.

Milly, P. C. D., Malyshev, S. L., Shevliakova, E., Dunne, K. A., Findell, K. L., Gleeson, T., Liang, Z., Phillips, P., Stouffer, R. J., and Swenson, S.: An enhanced model of land water and energy for global hydrologic and earth-system studies, J Hydrometeorol, 15, 1739-1761, doi: JHM-D-13-0162.1, 2014.

Mitchell, K. J.: Simulation of growth of even-aged stands of white spruce, Yale University School of Forestry Bulletin, 75, 1-48, 1969.

Moorcroft, P. R., Hurtt, G. C., and Pacala, S. W.: A method for scaling vegetation dynamics: The ecosystem demography model (ED), Ecol. Monogr., 71, 557-585, doi: 10.1890/0012-9615(2001)071[0557:AMFSVD]2.0.CO;2, 2001.

1170 Norby, R. J., and Zak, D. R.: Ecological Lessons from Free-Air CO2 Enrichment (FACE)
1171 Experiments, Annu. Rev. Ecol. Evol. S., 42, 181-203, doi: 10.1146/annurev-ecolsys-102209-
1172 144647, 2011.

1173 Pacala, S. W., Canham, C. D., Saponara, J., Silander, J. A., Kobe, R. K., and Ribbens, E.: Forest
1174 models defined by field measurements: Estimation, error analysis and dynamics, Ecol. Monogr.,
1175 66, 1-43, 1996.

1176 Pan, Y. D., Birdsey, R. A., Fang, J. Y., Houghton, R., Kauppi, P. E., Kurz, W. A., Phillips, O. L.,
1177 Shvidenko, A., Lewis, S. L., Canadell, J. G., Ciais, P., Jackson, R. B., Pacala, S. W., McGuire, A.
1178 D., Piao, S. L., Rautiainen, A., Sitch, S., and Hayes, D.: A Large and Persistent Carbon Sink in
1179 the World's Forests, Science, 333, 988-993, doi:10.1126/science.1201609, 2011.

1180 Parton, W. J., Schimel, D. S., Cole, C. V., and Ojima, D. S.: Analysis of Factors Controlling Soil
1181 Organic-Matter Levels in Great-Plains Grasslands, Soil Sci. Soc. Am. J., 51, 1173-1179, 1987.

1182 Poorter, L., and Arets, E. J. M. M.: Light environment and tree strategies in a Bolivian tropical
1183 moist forest: an evaluation of the light partitioning hypothesis, Plant Ecol., 166, 295-306, doi:
1184 10.1023/A:1023295806147, 2003.

1185 Potter, C. S., Randerson, J. T., Field, C. B., Matson, P. A., Vitousek, P. M., Mooney, H. A., and
1186 Klooster, S. A.: Terrestrial Ecosystem Production - a Process Model-Based on Global Satellite
1187 and Surface Data, Global Biogeochem. Cy., 7, 811-841, 1993.

1188 Prentice, I. C., Cramer, W., Harrison, S. P., Leemans, R., Monserud, R. A., and Solomon, A. M.:
1189 A Global Biome Model Based on Plant Physiology and Dominance, Soil Properties and Climate,
1190 J. Biogeogr., 19, 117-134, 1992.

1191 Purves, D. W., Lichstein, J. W., and Pacala, S. W.: Crown plasticity and competition for canopy
1192 space: A new spatially implicit model parameterized for 250 North American tree species, Plos
1193 One, 2, ARTN e870, doi: 10.1371/journal.pone.0000870, 2007.

1194 Purves, D. W., Lichstein, J. W., Strigul, N., and Pacala, S. W.: Predicting and understanding
1195 forest dynamics using a simple tractable model, P. Natl. Acad. Sci. USA, 105, 17018-17022,
1196 doi:10.1073/pnas.0807754105, 2008.

1197 Quillet, A., Peng, C. H., and Garneau, M.: Toward dynamic global vegetation models for
1198 simulating vegetation-climate interactions and feedbacks: recent developments, limitations, and
1199 future challenges, Environ. Rev., 18, 333-353, doi:10.1139/A10-016, 2010.

1200 Runkle, J. R.: Canopy tree turnover in old-growth mesic forests of eastern North America,
1201 Ecology, 81, 554-567, 2000.

1202 Ryan, M. G., Binkley, D., Fownes, J. H., Giardina, C. P., and Senock, R. S.: An experimental
1203 test of the causes of forest growth decline with stand age, Ecol. Monogr., 74, 393-414, 2004.

Sato, H., Itoh, A., and Kohyama, T.: SEIB-DGVM: A new dynamic global vegetation model using a spatially explicit individual-based approach, Ecol. Model., 200, 279-307, doi:10.1016/j.ecolmodel.2006.09.006, 2007.

Scheiter, S., Langan, L., and Higgins, S. I.: Next-generation dynamic global vegetation models: learning from community ecology, New Phytol., 198, 957-969, doi:10.1111/Nph.12210, 2013.

Shao, P., Zeng, X. B., Sakaguchi, K., Monson, R. K., and Zeng, X. D.: Terrestrial carbon cycle: climate relations in eight CMIP5 earth system models, J. Climate, 26, 8744-8764, doi:10.1175/Jcli-D-12-00831.1, 2013.

Sheffield, J., Goteti, G., and Wood, E. F.: Development of a 50-year high-resolution global dataset of meteorological forcings for land surface modeling, J. Climate, 19, 3088-3111, doi:10.1175/Jcli3790.1, 2006.

Shevliakova, E., Pacala, S. W., Malyshev, S., Hurtt, G. C., Milly, P. C. D., Caspersen, J. P., Sentman, L. T., Fisk, J. P., Wirth, C., and Crevoisier, C.: Carbon cycling under 300 years of land use change: Importance of the secondary vegetation sink, Global Biogeochem. Cy., 23, GB2022, doi:10.1029/2007gb003176, 2009.

Shinozaki, K., Yoda, K., Hozumi, K., and Kira, T.: A quantitative analysis of plant form - the pipe model theory I. Basic analysis, Jap. J. Ecol., 14, 97-106, 1964.

Shugart, H. H., and West, D. C.: Development of an Appalachian Deciduous Forest Succession Model and Its Application to Assessment of Impact of Chestnut Blight, J. Environ. Manage., 5, 161-179, 1977.

Shugart, H. H.: A theory of forest dynamics : the ecological implications of forest succession models, Springer-Verlag, New York, xiv, 278 p. pp., 1984.

Sillett, S. C., Van Pelt, R., Koch, G. W., Ambrose, A. R., Carroll, A. L., Antoine, M. E., and Mifsud, B. M.: Increasing wood production through old age in tall trees, For. Ecol. Manage., 259, 976-994, doi:10.1016/j.foreco.2009.12.003, 2010.

Sitch, S., Smith, B., Prentice, I. C., Arneth, A., Bondeau, A., Cramer, W., Kaplan, J. O., Levis, S., Lucht, W., Sykes, M. T., Thonicke, K., and Venevsky, S.: Evaluation of ecosystem dynamics, plant geography and terrestrial carbon cycling in the LPJ dynamic global vegetation model, Global Change Biol., 9, 161-185, 2003.

Sitch, S., Huntingford, C., Gedney, N., Levy, P. E., Lomas, M., Piao, S. L., Betts, R., Ciais, P., Cox, P., Friedlingstein, P., Jones, C. D., Prentice, I. C., and Woodward, F. I.: Evaluation of the terrestrial carbon cycle, future plant geography and climate-carbon cycle feedbacks using five Dynamic Global Vegetation Models (DGVMs), Global Change Biol., 14, 2015-2039, doi:10.1111/j.1365-2486.2008.01626.x, 2008.

Smith, B., Prentice, I. C., and Sykes, M. T.: Representation of vegetation dynamics in the modelling of terrestrial ecosystems: comparing two contrasting approaches within European

climate space, Global Ecol. Biogeogr., 10, 621-637, doi:10.1046/j.1466-822X.2001.t01-1-00256.x, 2001.

Snell, R. S., Huth, A., Nabel, J. E. M. S., Bocedi, G., Travis, J. M. J., Gravel, D., Bugmann, H., Gutierrez, A. G., Hickler, T., Higgins, S. I., Reineking, B., Scherstjanoi, M., Zurbriggen, N., and Lischke, H.: Using dynamic vegetation models to simulate plant range shifts, Ecography, 37, 1184–1197, 2014.

Strigul, N., Pristinski, D., Purves, D., Dushoff, J., and Pacala, S.: Scaling from Trees to Forests: Tractable Macroscopic Equations for Forest Dynamics, Ecol. Monogr., 78, 523-545, 2008.

Thornton, P. E., Lamarque, J. F., Rosenbloom, N. A., and Mahowald, N. M.: Influence of carbon-nitrogen cycle coupling on land model response to CO2 fertilization and climate variability, Global Biogeochem. Cy., 21, GB4018, doi:10.1029/2006gb002868, 2007.

Todd-Brown, K. E. O., Randerson, J. T., Post, W. M., Hoffman, F. M., Tarnocai, C., Schuur, E. A. G., and Allison, S. D.: Causes of variation in soil carbon simulations from CMIP5 Earth system models and comparison with observations, Biogeosciences, 10, 1717-1736, doi:10.5194/bg-10-1717-2013, 2013.

Valladares, F., Gianoli, E., and Gomez, J. M.: Ecological limits to plant phenotypic plasticity. New Phytol., 176, 749–763, 2007.

von Foerster, H.: Some remarks on changing populations, in: The kinetics of cellular proliferation, edited by: Stohlman, F. J., Grune and Stratton, New York, 382-407, 1959.

Wang, C. K.: Biomass allometric equations for 10 co-occurring tree species in Chinese temperate forests, For. Ecol. Manage., 222, 9-16, doi:10.1016/j.foreco.2005.10.074, 2006.

Weng, E. S., and Luo, Y. Q.: Relative information contributions of model vs. data to short- and long-term forecasts of forest carbon dynamics, Ecological Applications, 21, 1490-1505, 2011.

Weng, E. S., Luo, Y. Q., Wang, W. L., Wang, H., Hayes, D. J., McGuire, A. D., Hastings, A., and Schimel, D. S.: Ecosystem carbon storage capacity as affected by disturbance regimes: A general theoretical model, J. Geophys. Res., 117, G03014, doi:10.1029/2012jg002040, 2012.

Woods, K. D.: Dynamics in late-successional hemlock-hardwood forests over three decades, Ecology, 81, 110-126, 2000.

Wullschleger, S. D., Epstein, H. E., Box, E. O., Euskirchen, E. S., Goswami, S., Iversen, C. M., Kattge, J., Norby, R. J., van Bodegom, P. M., and Xu, X. F.: Plant functional types in Earth system models: past experiences and future directions for application of dynamic vegetation models in high-latitude ecosystems, Ann. Bot., 114, 1-16, doi:10.1093/Aob/Mcu077, 2014.

Xu, C. Y., Turnbull, M. H., Tissue, D. T., Lewis, J. D., Carson, R., Schuster, W. S. F., Whitehead, D., Walcroft, A. S., Li, J. B., and Griffin, K. L.: Age-related decline of stand biomass accumulation is primarily due to mortality and not to reduction in NPP associated with individual

tree physiology, tree growth or stand structure in a Quercus-dominated forest, J. Ecol., 100, 428-440, doi:10.1111/j.1365-2745.2011.01933.x, 2012.

Yang, Y. H., Luo, Y. Q., and Finzi, A. C.: Carbon and nitrogen dynamics during forest stand development: a global synthesis, New Phytol., 190, 977-989, doi:10.1111/j.1469-8137.2011.03645.x, 2011.

Zachos, J., Pagani, M., Sloan, L., Thomas, E., and Billups, K.: Trends, rhythms, and aberrations in global climate 65 Ma to present, Science, 292, 686–693, 2001.

Zaehle, S., and Friend, A. D.: Carbon and nitrogen cycle dynamics in the O-CN land surface model: 1. Model description, site-scale evaluation, and sensitivity to parameter estimates, Global Biogeochem. Cy., 24, GB1005, doi:10.1029/2009gb003521, 2010.

Zea-Cabrera, E., Iwasa, Y., Levin, S., and Rodriguez-Iturbe, I.: Tragedy of the commons in plant water use, Water Resour. Res., 42, W06d02, doi:10.1029/2005wr004514, 2006.

Zhang, L., Luo, Y. Q., Yu, G. R., and Zhang, L. M.: Estimated carbon residence times in three forest ecosystems of eastern China: Applications of probabilistic inversion, J. Geophys. Res., 115, G01010, doi:10.1029/2009jg001004, 2010.

Zhang, T., Lichstein, J. W., and Birdsey, R. A.: Spatial and temporal heterogeneity in the dynamics of eastern U.S. forests: Implications for developing broad-scale forest dynamics models, Ecol. Model., 279, 89-99, doi: 10.1016/j.ecolmodel.2014.02.011, 2014.

Table 1. Parameter values for the three tree species in the LM3-PPA simulations presented in Figs. 2-7.

Parameter	Definition and unit	Trembling aspen (*Populus tremuloides*)	Sugar maple (*Acer saccharum*)	Red maple (*Acer rubrum*)
N_0^*	Initial density (individuals ha^{-1})	1500	200	70
Λ	taper factor of trees	0.65	0.65	0.65
α_Z	Scaling parameter of tree height with DBH	36.01	36.41	36.41
α_C	Scaling parameter of crown area with DBH	140	150	150
φ_{CSA}	Ratio of sapwood cross section area to target leaf area	2.5×10^{-4}	2.5×10^{-4}	2.5×10^{-4}
φ_{RL}	Ratio of fine root surface area to leaf area	0.8	0.8	0.8
LMA	Leaf mass per unit of area (kg C m^{-2})	0.0445	0.035	0.038
l^*	target crown LAI	3.0	3.8	3.5
μ_{C0}	Background mortality rate (yr^{-1}) of canopy trees	0.065	0.012	0.020
μ_{U0}	Minimum background mortality rate (yr^{-1}) of understory trees (see Table 2)	0.162	0.049	0.081
$V_{cmax,\,0}$	maximum rate of carboxylation at 25° C (mol CO_2 m^{-2} s^{-1})	30.0 E-6	22.0 E-6	25.0 E-6
f_{WF}	Conversion rate of C in NSC to woody tissues and seeds (fraction d^{-1})	3.425×10^{-3}	1.096×10^{-3}	1.096×10^{-3}

ρ_W	wood density (kg C m^{-3})	230	265	255

[*]Initial densities in Table 1 are approximate and are summed across size classes. See Table C4 in Appendix C for details of the initial size distributions used in the simulations.

Table 2. Parameters for alternative assumptions regarding crown-area allometry and mortality of large trees, and gap dynamics (canopy-space-filling). Model H0 is the baseline LM3-PPA model, and H1-H3 are alternative models.

Model	$\theta_{C,D<0.8m}$	$\theta_{C,D\geq0.8m}$	μ_C	Gap dynamics
H0	1.5	1.5	μ_{C0}	Tallest
H1	1.5	1.5	$\mu_{C0}\left[\frac{1+10e^{15(D-D\mu_C)}}{1+e^{15(D-D\mu_C)}}\right]$	Tallest
H2	1.5	0.0	μ_{C0}	Tallest
H3	1.5	1.5	μ_{C0}	Randomly selected

Notes:

$\theta_{C,D<0.8m}$ and $\theta_{C,D\geq0.8m}$ are the exponents in the crown area allometry (Eq 4) for trees with DBH < 0.8 and ≥ 0.8 m, respectively.

$D\mu_C$ = 1.0 m

The "gap dynamics" algorithm labeled "Tallest" is the standard PPA assumption, in which the tallest understory trees fill the space vacated by the death of canopy trees (H0-H2, Strigul et al., 2008). The alternative assumption ("Randomly selected") selects understory trees at random (regardless of their height) to fill this vacated space (H3).

Table 3. Experimental design for model runs used to identify fine-root allocation strategies that are competitively optimal (evolutionarily stable strategies, ESSs) and that maximize wood production in monoculture. In these experiments, the plant functional types (PFTs) varied only in the ratio of fine-root surface area to leaf area (φ_{RL}). Because all PFTs shared the same target crown LAI, the parameter φ_{RL} primarily controls allocation to fine roots and wood.

	Model runs	Initial PFT(s) (φ_{RL})	Initial density (seedling ha^{-1})	Invading PFT (φ_{RL})	[CO_2] (ppm)
Polyculture	2	0.5, 0.6, 0.7, 0.8, 0.9	50 for each PFT	none	280/ 560
Monoculture	2 per PFT	0.5, 0.6, 0.7, 0.8, 0.9	250	none	280/ 560
Invasion	1	0.6	250	0.7	280
	2	0.7	250	0.6	280
				0.9	
	1	0.7	250	0.9	560
	2	0.9	250	0.7	560
				1.0	

Figure legends

Figure 1. Scaling of mortality rates (a) and tree height and crown area (b) with DBH in four alternative versions of the LM3-PPA model (H0-H3; see Table 2).

In panel a, the solid line shows the mortality rates of understory trees (same for H0-H3); the dashed line shows the mortality rates of canopy trees in H0, H2, and H3; and the dotted line is for canopy trees in H1. In panel b, the solid line is tree height (same for H0-H3); the dashed line shows crown area in H0, H1, and H3; and the dotted line is crown area in H2.

Figure 2. GPP, NPP, allocation, and DBH growth rate

Panel a shows GPP (closed circles) and NPP (open circles) simulated by LM3-PPA for one species (sugar maple) in the 1° × 1° grid cell containing the Willow Creek Ameriflux site in Wisconsin, USA. The red open circles with error bars are GPP estimates from the Willow Creek eddy flux data (Desai et al. 2005). The red open diamond is NPP estimated from biometric data at Willow Creek (Curtis et al. 2002). Panel b shows the simulated allocation of NPP to leaves, fine roots, woody tissues (including stems, branches, and coarse roots), and seeds. The green open circle, red open triangle, and black open circle are NPP of wood, fine roots, and leaves, respectively, estimated from biometric data (Curtis et al. 2002). Panel c shows the DBH growth rates of canopy trees (closed circles) and understory trees (open circles) simulated for sugar maple. The red circle and diamond show growth rates of canopy and understory trees for sugar maple in the northern Lake States, USA estimated from FIA forest inventory data (Zhang et al. 2014). The error bars represent one standard deviation.

Figure 3. Simulated vs. observed DBH growth rates of three tree species in the upper canopy and the understory.

Circles, triangles, and diamonds are for *Populus tremuloides*, *Acer saccharum*, and *A. rubrum*, respectively. Closed and open symbols are for upper-canopy ("Top") and understory ("Under") trees, respectively. The FIA data used to estimate observed growth rates are from the northern Lake States (Michigan, Wisconsin, and Minnesota), USA. Canopy growth rates were estimated by combining trees with a reported crown class of "dominant" or "co-dominant", and understory growth rates were estimated from trees with a crown class of "overtopped" (Zhang et al., 2014).

Figure 4. Forest succession

Panel a shows simulated forest succession for three species (*Populus tremuloides*, *Acer saccharum*, and *A. rubrum*), with parameters and initial densities in Table 1. Panel b shows the successional dynamics estimated from FIA inventory data in the northern Lake States, USA. The basal areas of the three species are normalized relative to the maximum of their summed basal areas because the three species in the model runs account for only approximately one half of the total basal area in the data. This normalization only changes the y-axis scale. The non-normalized predictions and data are in Fig. S5, Supplemental materials.

Figure 5. Distributions of tree size (a) and biomass (b) in different stand age classes.

Black signs with dashed lines are from the FIA data of the northern Lake States, USA, and blue signs with solid lines are from the three-species LM3-PPA simulations in Fig. 4a.

Figure 6. Simulated distributions of tree size and biomass at quasi-equilibrium in one-species (*Acer saccharum*) LM3-PPA simulations under alternative models assumptions (H0-H3).

Size and biomass distributions are averaged over the last 400 years of 1000-year simulations. a: Tree density of trees in 10-cm DBH bins. b: Total tree density and basal area, summed over the size distribution in panel a. The error bars represent one standard deviation. c: Woody biomass in 10-cm DBH bins. Different colors in the figure refer to differ alternative model assumptions (see Table 2 and Fig. 1 for details): H0 is the baseline LM3-PPA model; H1 assumes that mortality rate increases with size for large trees; H2 assumes a maximum individual crown area, which causes a decline in DBH growth rate for large trees; and H3 assumes that open canopy space is filled by randomly chosen understory trees, rather than the tallest understory trees as in the PPA model.

Figure 7. Simulated dynamics of biomass (a), soil carbon (b), and biomass turnover rate (c) in LM3-PPA and in a standard biogeochemical cycle (BGC) model that does not represent individual-level processes.

LM3-PPA was simulated with either one species (*Acer saccharum*) or all three species in Table 1 and Fig. 4a. The standard BGC model is summarized in Fig. S1b in Supplemental materials.

Figure 8. Competition among PFTs that differ only their allocation to fine roots.

Competition experiments were performed at two atmospheric CO_2 concentrations, 280 ppm (a) and 560 ppm (b). In each experiment, a simulation was initialized with equal seedling densities

of five PFTs that differed only in their ratio of fine-root area to leaf area (φ_{RL}). Because all PFTs shared the same target crown LAI, φ_{RL} primarily determines allocation to fine roots and wood.

Figure 9. DBH growth rates of residents and invaders in pairwise invasion simulations. This figure shows DBH growth rates in pairwise competition experiments at (a) pre-industrial [CO_2] (280 ppm) and (b) doubled [CO_2] (560 ppm) for residents (black bars) and invaders (gray bars) that differed only in their fine-root allocation (φ_{RL}; see Fig. 8 legend for explanation). In each experiment, the resident type was simulated for 400 years in monoculture, and then a small fraction of its density was converted to the invading type. The competitive optimum (φ_{RL} = 0.7 and φ_{RL} = 0.9 at 280 ppm and 560 ppm, respectively) is the type (φ_{RL}) that cannot be invaded and can invade all other types (i.e., the convergence-stable evolutionarily stable strategy, ESS).

Figure 10. Woody NPP and DBH growth rates in monoculture and polyculture models runs at (a-b) [CO_2] = 280 ppm, and (c-d) [CO_2] = 560 ppm. PFTs differed only their allocation to fine roots (φ_{RL}; see Fig. 8 legend for explanation). The optimal monoculture is defined as the type with the highest woody NPP (which, given the allometries in LM3-PPA, is also the type with the highest DBH growth rate) when grown in monoculture. In this figure, the competitive optimum is identified as the type with the highest woody NPP (or highest DBH growth rate) in polyculture model runs. Figures 8-10 present multiple ways to identify the competitive optimum (i.e., the convergence-stable ESS), and all yield consistent results: φ_{RL} = 0.7 and φ_{RL} = 0.9 at 280 ppm and 560 ppm, respectively.

Figure 11. Changes in wet period length, water use efficiency (WUE), hydrological fluxes, and soil moisture due to a doubling of atmospheric CO_2 concentration.

The bars show the percentage differences between LM3-PPA run with a single PFT (φ_{RL}=0.7) at $[CO_2]$ = 560 ppm and at preindustrial $[CO_2]$ (280 ppm). The "Wet season" bar shows the effect of a doubling of preindustrial $[CO_2]$ on the fraction of each growing season in which canopy trees in the monoculture simulation are water-saturated (defined as the fraction of days during the growing season in which water supply was greater than or equal to demand at 2:00 p.m. over the final 60 years of a 500-year run). The "WUE" bar shows the change in the water use efficiency of canopy trees during the water-limited period (days in which water supply was less than demand at 2:00 p.m.). The "Transp" and "Evap+Runoff" bars show the changes in water transpired by plants and lost via evaporation and runoff over the last 60 years of the model runs; when expressed in absolute amounts (mm yr^{-1}), the decrease in transpiration and the increase in evaporation plus runoff almost exactly cancel each other (see section 3.3 in Results). The "Soil moisture" bar shows change in growing-season mean soil moisture at doubled CO_2.

1422 **Figure 1**

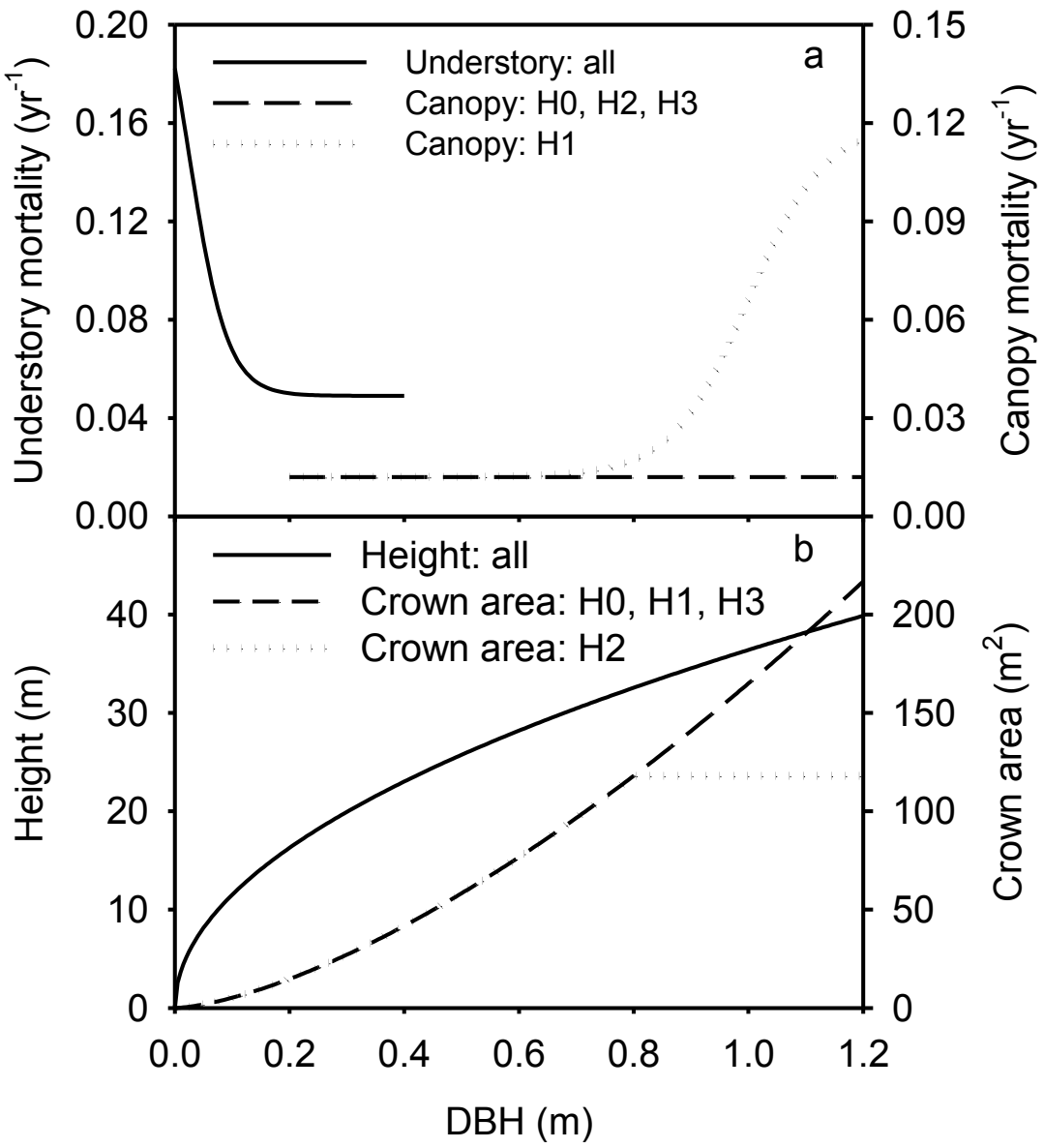

1423

1424

1425

1426 **Figure 2**

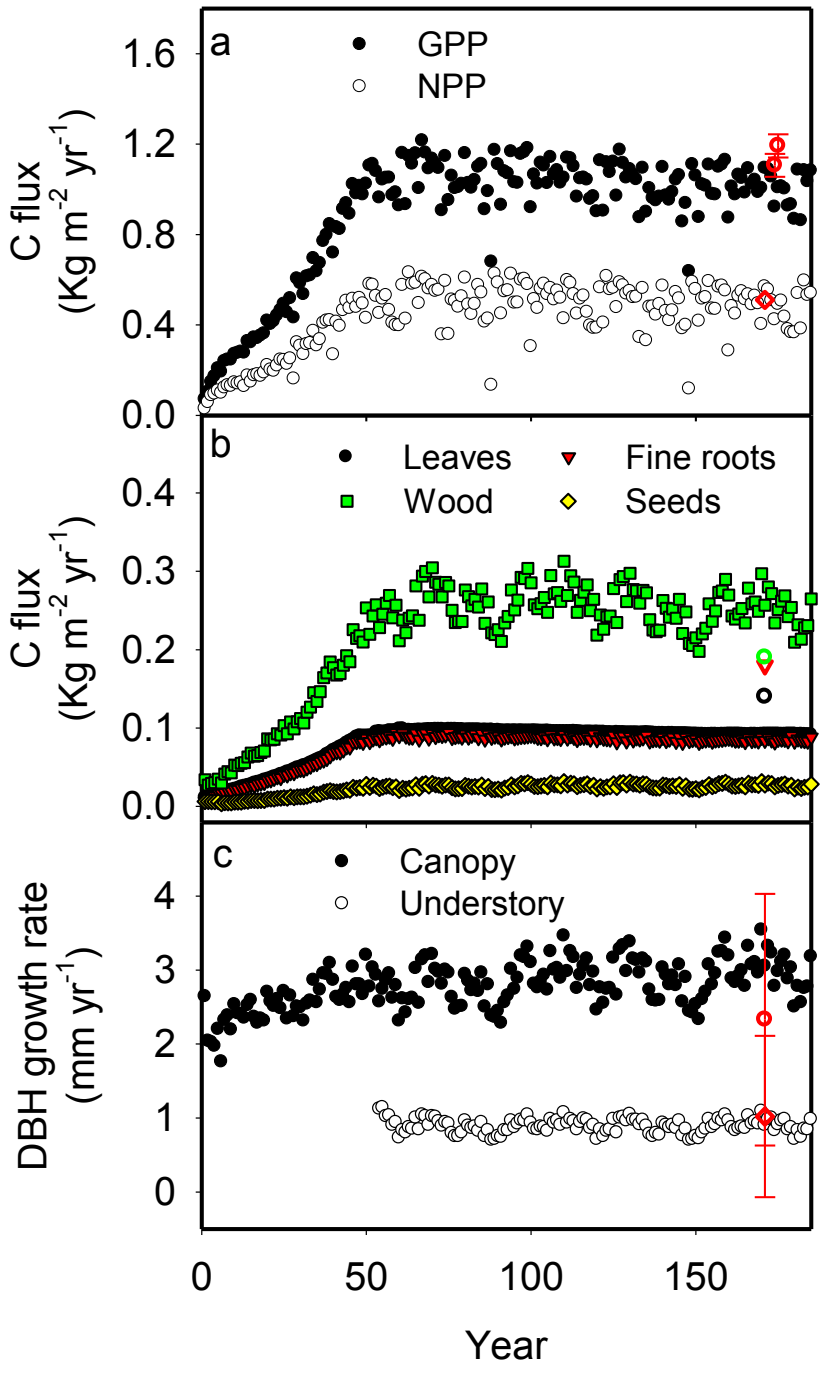

1427

1428

1429

1430 **Figure 3**

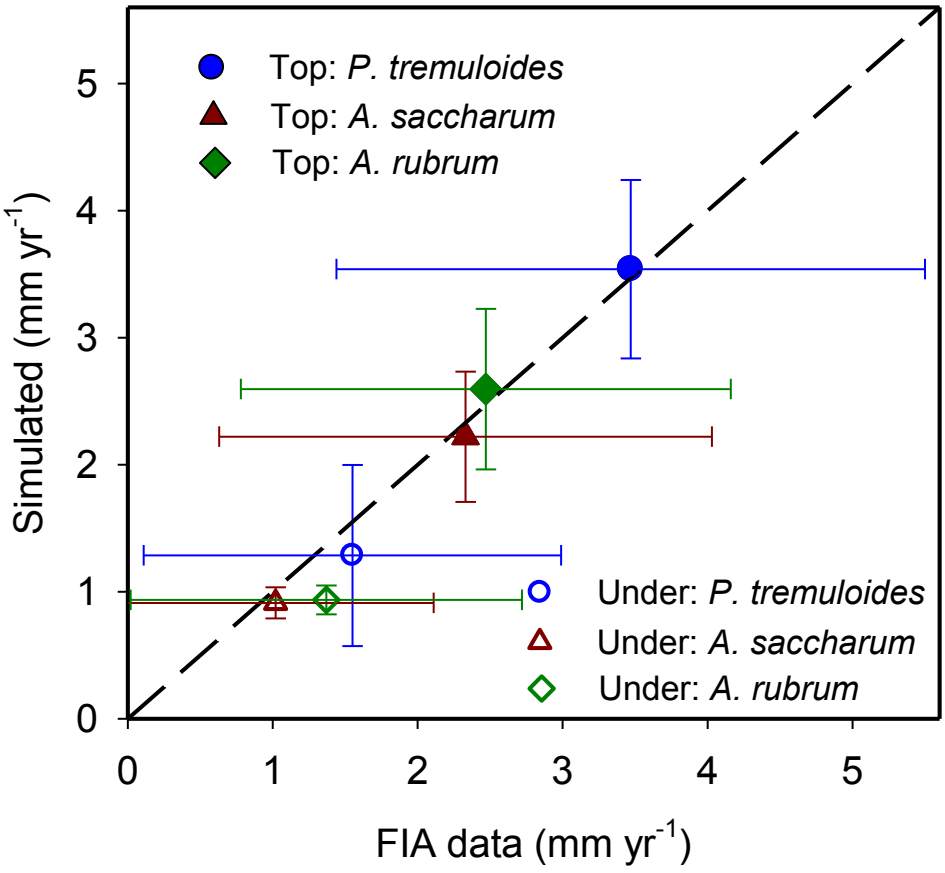

1431

1432

1433

1434 **Figure 4**

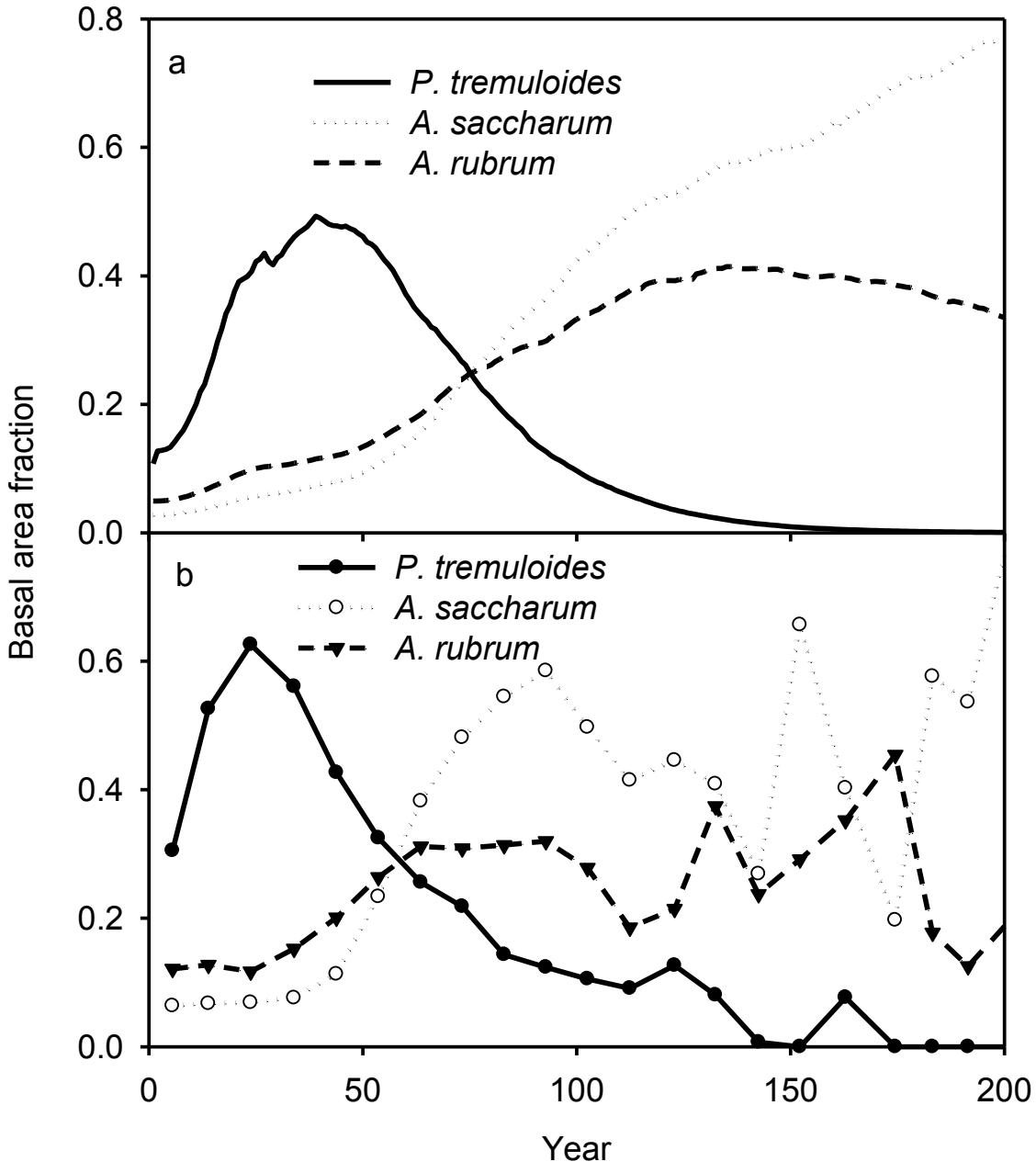

1435

1436

1437

1438 **Figure 5**

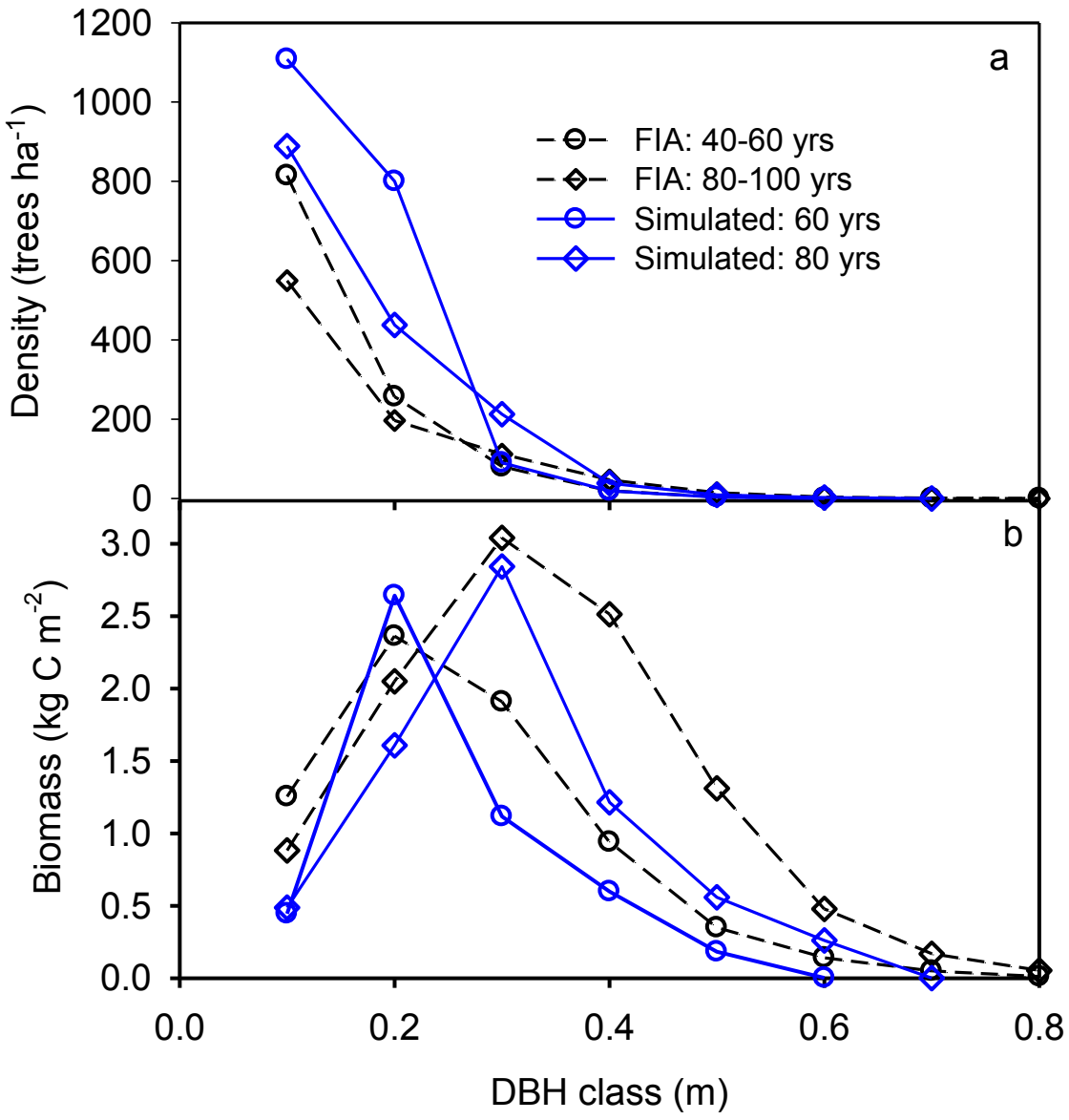

1439

1440

1441

1442 **Figure 6**

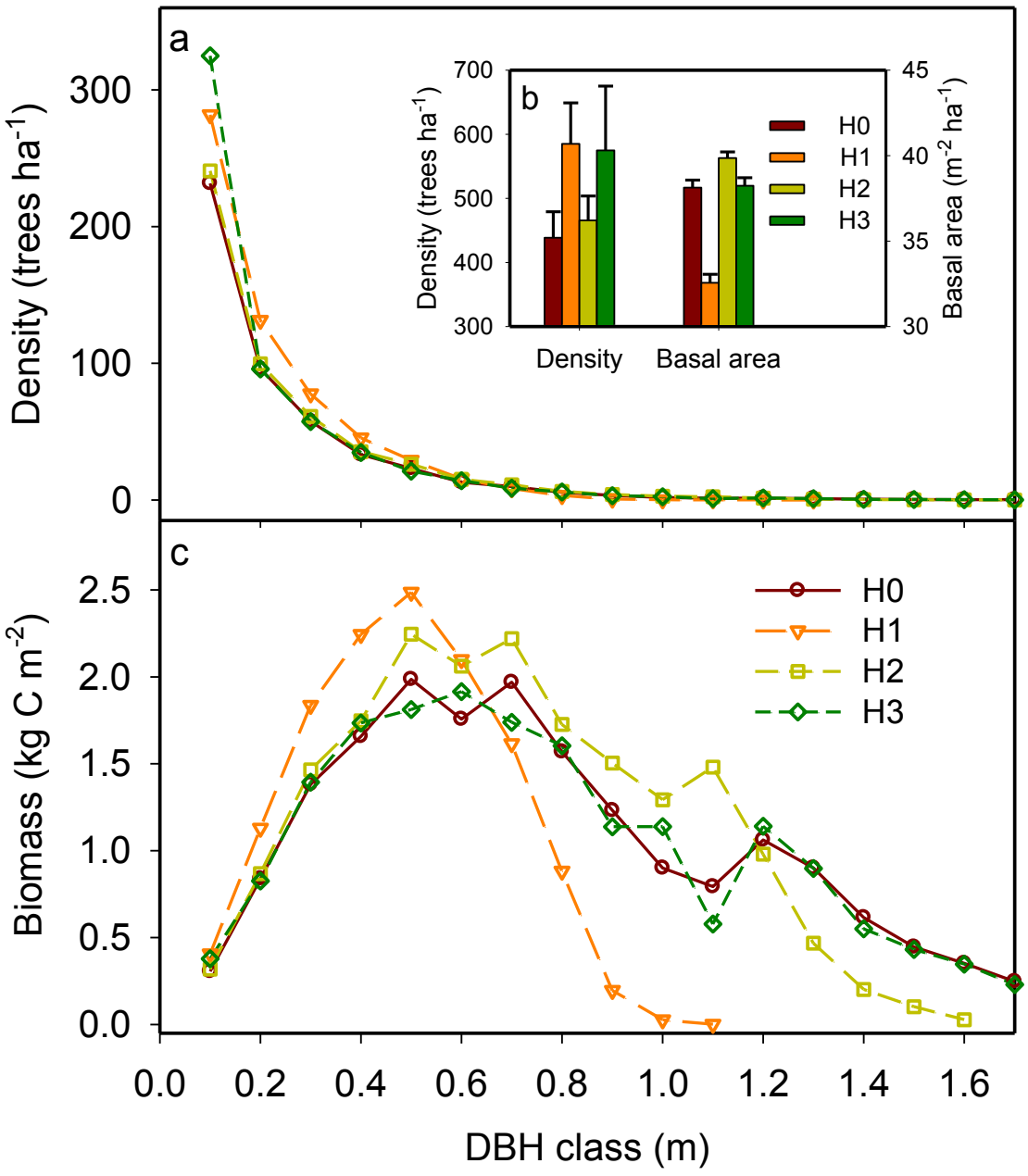

1443

1444

1445

1446 **Figure 7**

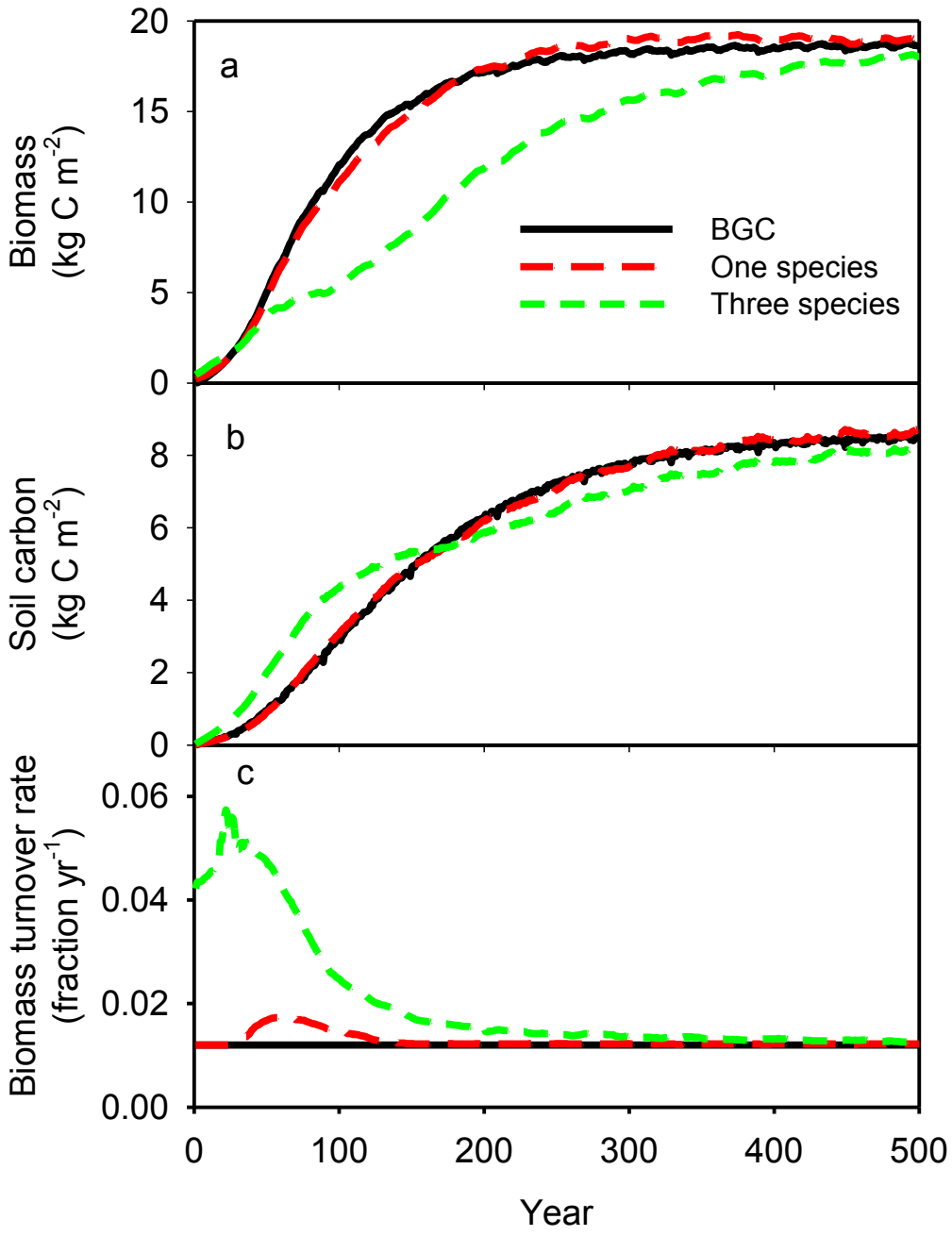

1447

1448

1449

1450 **Figure 8**

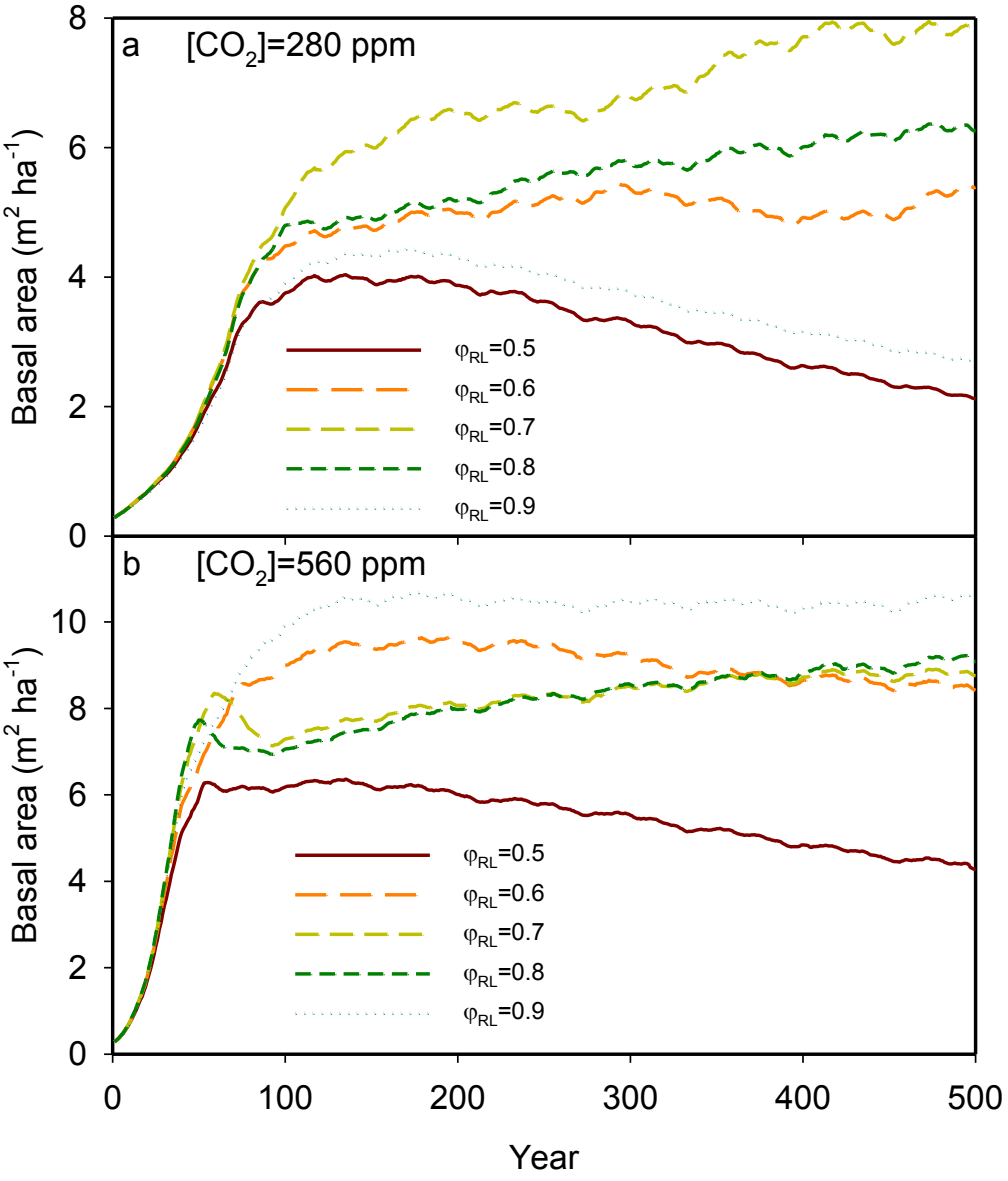

1451

1452

1453

1454 **Figure 9**

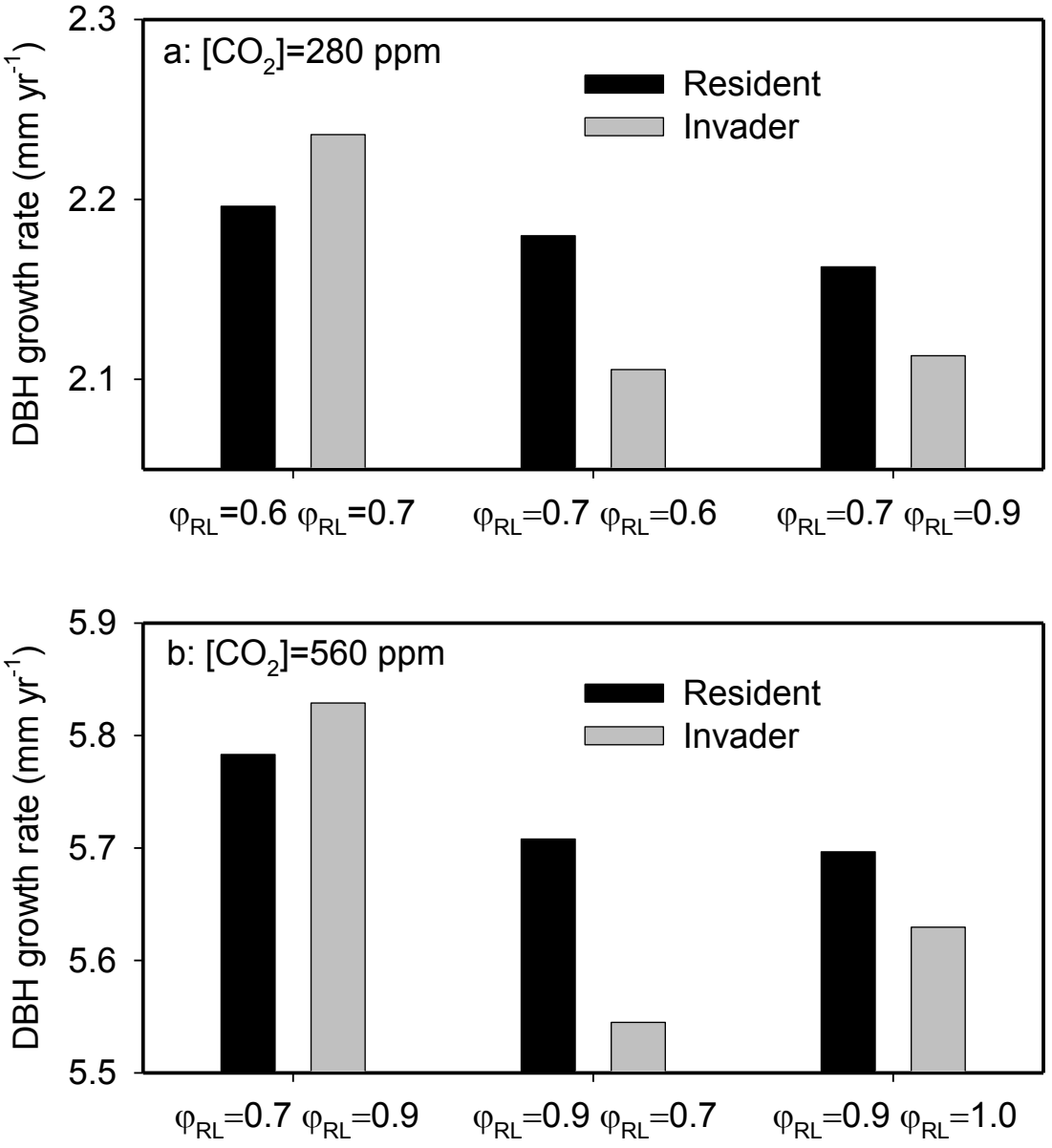

1455

1456

1457

1458 **Figure 10**

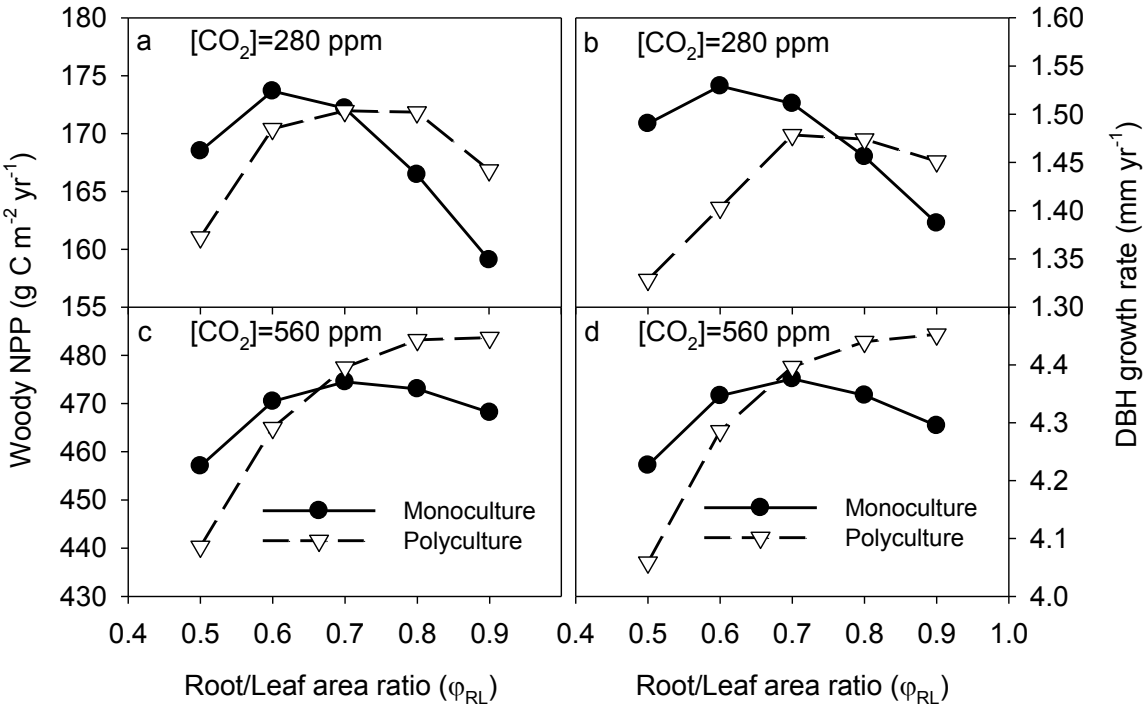

1459

1460

1461

1462 **Figure 11**

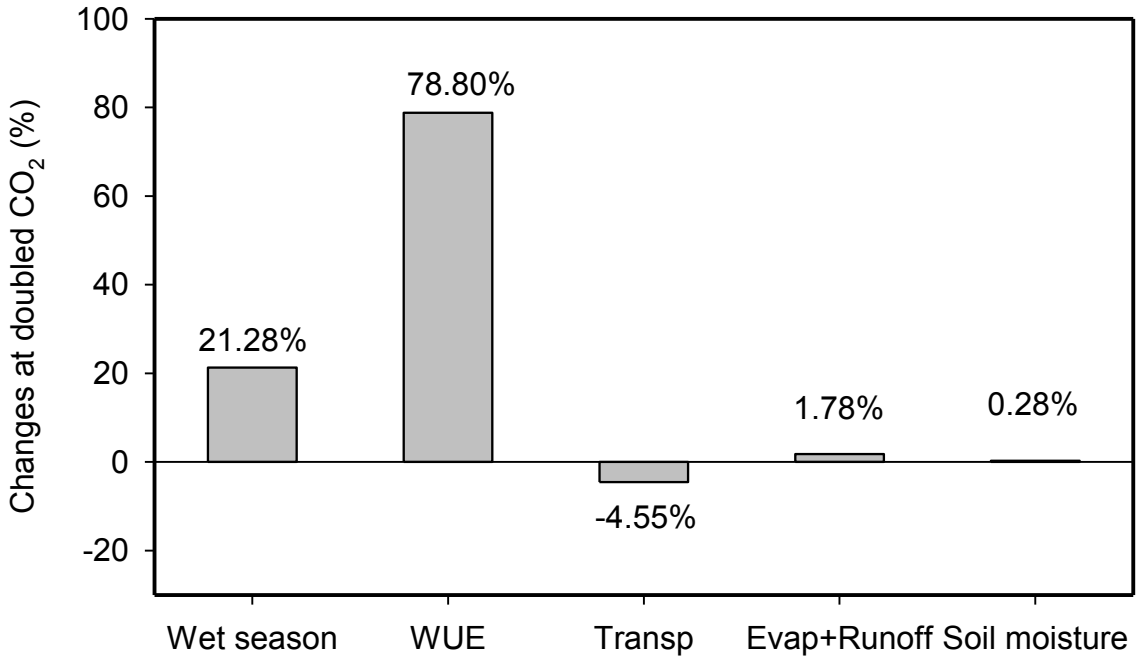

1463
1464